JOURNAL OF GEOPHYSICAL RESEARCH, VOL. 115, D11114, doi:10.1029/2009JD013204, 2010

Click Here for Full Article

Real-time weekly global green vegetation fraction derived from advanced very high resolution radiometer-based NOAA operational global vegetation index (GVI) system

Le Jiang,[1] Felix N. Kogan,[2] Wei Guo,[1] J. Dan Tarpley,[2] Kenneth E. Mitchell,[3] Michael B. Ek,[3] Yuhong Tian,[1] Weizhong Zheng,[4] Cheng-Zhi Zou,[2] and Bruce H. Ramsay[2]

Received 14 September 2009; revised 22 December 2009; accepted 20 January 2010; published 15 June 2010.

[1] To provide quality-improved and consistent real-time global green vegetation fraction (GVF) data products that are suitable for use in operational numerical weather, climate, and hydrological models, necessary processing steps are applied to the output data stream from the advanced very high resolution radiometer (AVHRR)-based NOAA operational global vegetation index (GVI) system. This paper reviewed the NOAA GVI data and described the algorithm to derive weekly updated real-time GVF from the normalized difference vegetation index (NDVI). The methodology description focuses on algorithm justification in an operational production context. The described algorithm was implemented in the global vegetation processing system (GVPS). The new global GVF data sets include the multiyear GVF weekly climatology and the real-time weekly GVF. Compared to the old 5 year GVF monthly climatology currently used in the operational National Centers for Environmental Prediction (NCEP)/Environmental Modeling Center (EMC) weather and climate models, the new data sets provide an overall higher vegetation value, real-time surface vegetation information, and numerous other improvements. The new GVF data set quality was partially assured by validation against Moderate Resolution Imaging Spectroradiometer (MODIS) NDVI at a few EOS land validation core sites and comparison with another independently processed NDVI data set. Impact of the new GVF data sets in numerical weather prediction (NWP) model was investigated using EMC mesoscale model simulations and concluded overall positive.

Citation: Jiang, L., F. N. Kogan, W. Guo, J. D. Tarpley, K. E. Mitchell, M. B. Ek, Y. Tian, W. Zheng, C.-Z. Zou, and B. H. Ramsay (2010), Real-time weekly global green vegetation fraction derived from advanced very high resolution radiometer-based NOAA operational global vegetation index (GVI) system, *J. Geophys. Res.*, *115*, D11114, doi:10.1029/2009JD013204.

1. Introduction

[2] Operational numerical weather prediction (NWP) centers have come to rely on global estimates of seasonally varying vegetation cover in surface energy balance physics in the forecast models. In the global and regional NWP models of the National Centers for Environmental Prediction (NCEP), green vegetation fraction (GVF) is used to partition the fraction of the surface in the model grid cell, which is evaporating at rates controlled by vegetation as opposed to the fraction evaporating as a bare soil surface. The surface energy and moisture balances in NWP models are very sensitive to GVF [*Abramopoulos et al.*, 1988]. Early tests with one of NOAA's operational regional models, the Eta model, showed significant improvement in forecasts of surface evaporation and low-level humidity and temperature by using the 5 year mean monthly GVF climatology [*Betts et al.*, 1997]. Such a 5 year GVF climatology [*Gutman and Ignatov*, 1998] is presently used by NCEP operational NWP models. It has the spatial-temporal resolution of 0.144° (approximately 16 km at the equator) monthly, and it is in a latitude-longitude projection, derived from five selected optimum years of the advanced very high resolution radiometer (AVHRR) -based operational NOAA global vegetation index (GVI) product [*Kidwell*, 1994, 1997], namely, April 1985 to March 1991, with year 1988 excluded due to deterioration of data following a severe drifting in NOAA-9 satellite orbit. This monthly climatology describes the seasonality of GVF, which was useful to the NWP models. The 5 year AVHRR

[1]I. M. Systems Group, Inc., National Environmental Satellite, Data, and Information Service, NOAA, Camp Springs, Maryland, USA.
[2]National Environmental Satellite, Data, and Information Service, Center for Satellite Applications and Research, NOAA, Camp Springs, Maryland, USA.
[3]National Centers for Environmental Prediction, Environmental Modeling Center, NOAA, Camp Springs, Maryland, USA.
[4]Science Applications International Corporation, National Centers for Environmental Prediction, Environmental Modeling Center, NOAA, Camp Springs, Maryland, USA.

Copyright 2010 by the American Geophysical Union.
0148-0227/10/2009JD013204

GVF climatology was implemented operationally in the NCEP mesoscale NWP models in February 1997 [*Ek et al.*, 2003].

[3] The 5 year monthly GVF climatology is based on top-of-atmosphere (TOA) monthly average normalized difference vegetation index (NDVI), which was derived from post launch-calibrated [*Rao and Chen*, 1995] and cloud-screened [*Gutman et al.*, 1994] weekly composite AVHRR data. A 3 × 3 pixels mean spatial filter was applied to further reduce residual cloud and fill gaps on the NDVI map. Then the monthly averaged NDVI was used to derive monthly GVF using a linear equation [*Gutman and Ignatov*, 1998]. For each month, both the 5 year mean and standard deviation of GVF were calculated for each pixel. This climatology captures the major global seasonal variation and geographic distribution of GVF with 12 separate monthly global data fields for an annual cycle.

[4] Although in the past this GVF data set made significant improvements to the NCEP forecasts, further improvements are needed. The key issue remains that the GVF climatology (thus static for the same month of different years) lacks the ability to capture real-time vegetation status while only prescribing the multiannual mean. In addition, the spatial smoothing in this GVF product generation somewhat reduced the effective resolution. Heterogeneous land surface conditions within the 3 × 3 0.144° resolution pixels may have different annual cycles of natural land cover growth (such as desert, grassland, forest, etc.); thus, spatial smoothing is not desirable. Further, the monthly temporal aggregation may bias the spatial relationship between neighboring pixels because different vegetation types have different characteristic seasonal growth patterns. Since phenological changes and leaf appearances can occur every 3–7 days, the 1 month period is too long to accurately characterize development of vegetation [*Ulanova*, 1975]. Under a severe drought event, land surface vegetation can be desiccated in days, which implies that tracking vegetation change on a monthly basis is not sufficient [*Kogan*, 1997]. The 5 year monthly GVF climatology currently used in the NCEP operational models may miss an earlier or later spring vegetation green up or changes in GVF due to drought or excessively wet conditions. Another limitation with this climatology is that only 5 years' data were used, thus having a low statistical significance, although it was a practical approach given the limitation of the usable data amount at the time it was derived.

[5] The increasing need for a real-time GVF data set is driven by the requirement of accurate representation of land surface vegetation both spatially and temporally in the numerical models. The annual precipitation for a given region may have significant variation from year to year, especially in arid and semiarid areas. The real-time surface vegetation cover information will manifest interannual variability. It is required that NCEP has an improved operational GVF product, which reflects real-time conditions in vegetation dynamics showing droughts and moist conditions. The described new GVF product development in this paper is for the Noah land surface model (LSM), which was developed by the NCEP, Oregon State University, U.S. Air Force, and the NOAA Hydrologic Research Laboratory, and is used operationally in NCEP global and regional models [*Ek et al.*, 2003]. This LSM uses GVF to determine the fraction of the model over which vegetation is transpiring and the fraction of soil surface is exposed for direct evaporation. A real-time GVF can directly alter the partitioning of surface sensible and latent heat fluxes and can be particularly important to accurately predicting boundary layer structures [*Kurkowski et al.*, 2003]. It was further demonstrated that the use of near-real-time vegetation fraction provided more accurate forecasts of the environmental conditions such as the values and structure of low-level temperature and dew point temperature fields compared to forecasts using climatological vegetation fractions, and the environmental forecasts that resulted from using the real-time vegetation fraction are more thermodynamically supportive of convection [*James et al.*, 2009]. The Noah LSM has four soil layers for temperature and moisture and one canopy layer with canopy moisture and snow cover. It predicts soil moisture, soil temperature, skin temperature, snowpack depth, snowpack water equivalent, canopy water content, and the energy and water flux terms of the surface energy and water balances [*Mitchell et al.*, 2004]. It provides sensible and latent heat fluxes as the lower boundary condition for the vertical transport in the boundary layer scheme.

[6] Within the context of this paper, "real time" means "weekly" remaining with the operationally available GVI weekly composite of relevant AVHRR channels. Considering the operational constraints, we implement algorithms to take the GVI output data stream as input to derive quality-improved NDVI and then further derive GVF from NDVI. Our study here is focused on deriving weekly updated GVF meeting the "initial data" requirement by the weather forecasting community through an improved real-time GVF data set built on the existing NOAA operational data stream. This is different from other research groups that are developing physics-based algorithms and statistical procedures in a reprocessing mode, which is not real-time critical. The goal of this paper is to derive GVF from the existing GVI data stream; compare the new GVF data set against the old 5 year monthly GVF climatology currently used by NCEP/Environmental Modeling Center (EMC) models; assess the quality of the new GVF data with limited independent observations; and demonstrate the impact of new GVF data in EMC numerical models.

[7] Section 2 describes the data input as the basis of the current development and discusses several limitations in the GVI data sets. Section 3 clarifies the physical meaning of the GVF and describes the approach for deriving real-time GVF in the operational environment. Section 4 compares the new 24 year weekly GVF data sets and the old 5 year monthly GVF climatology. It also provides limited validation of GVF using MODIS-derived NDVI surrounding a few EOS land validation core sites and compares GVF with other independently derived AVHRR-based NDVI data set. It further demonstrates the impact of the new GVF data set in EMC models. Section 5 discusses the pros and cons of the current development, differences between reprocessing and operational real-time processing, and other limitations. Section 6 concludes this study.

2. Input Data Description

[8] For over two decades, NOAA has been operating the GVI system, which provides weekly composite AVHRR sensor (onboard NOAA polar orbiting satellites) channel counts for multiple channels, along with solar zenith angles

and satellite azimuth angles. A channel count is an 8-bit binary value to cover the digital range from 0 to 255. A predetermined set of coefficients are used to convert channel count into reflectance (which is the physical value). GVI is based on the weekly (i.e., 7 day) composite of daily global area coverage (GAC) data, which is a level 1B data set produced routinely with the highest resolution at 4 km (see *NOAA Polar Orbiter Data User's Guide* and *NOAA KLM User's Guide*, both available at http://www.ncdc.noaa.gov/oa/pod-guide/ncdc/docs). GVI resamples GAC daily data by extracting every fourth GAC line (in both dimensions; thus, it extracts the last pixel from the 4 × 4 GAC pixels array) and uses weekly maximum value composite (MVC) to remove cloud contamination based on the pixel's maximum NDVI. Strictly speaking, NDVI is defined as the difference between near-infrared (NIR) and visible (VIS) channel reflectances divided by the sum of the two, but for efficiency reasons, in GVI, it was calculated as the difference in two channel counts divided by the sum of channel counts during the compositing period [*Kidwell*, 1994, 1997]. GVI data products include weekly composites of AVHRR channels 1, 2, 3 (or 3a and 3b for later AVHRR sensors), 4, and 5 digital counts (but not channel reflectance), solar zenith angle, and relative azimuth angle at 0.144° resolution with a subglobal coverage from 75°N to 55°S. GVI also calculates NDVI, but it is only a "raw NDVI" since it is a quick estimation rather than an accurate calculation.

[9] The limitations in weekly produced GVI data sets are briefly discussed here. First, the NDVI data calculated in GVI is highly noisy and not applicable for numerical use due to the lack of post launch calibration and other corrections. However, it is useful in monitoring global vegetation patterns in real time. Second, the MVC scheme (used to produce these maps with reduced cloud contamination in GVI) cannot completely remove cloud effects if pixel level cloud cover persists longer than the 7 day compositing period. The residual cloud contamination remains a significant problem in the GVI products. The weekly MVC maps contain data from different days with varying atmospheric conditions such as column water vapor, ozone, aerosol profiles, and varying radiometric properties from the surface such as different Sun-target-sensor geometry and surface canopy bidirectional reflectance [*Roujean et al.*, 1992; *Huete et al.*, 1992]. It is recognized that well-investigated and physically based correction algorithms to AVHRR channel reflectances had not been developed at the time of GVI becoming mature and operational. These include those addressing instrument issues such as (1) satellite drift in the equator-crossing time of the orbit, which causes the local solar time of observation to vary by 3 h as the satellite ages; (2) variability in VIS band calibration over instrument life; (3) variations in VIS band spectral response and calibration from one AVHRR instrument to the next; and (4) atmospheric contamination such as ozone, Rayleigh scattering, aerosol, and water vapor, as well as the directional reflectance differences. However, even with the lack of operational algorithms to correct these issues, NDVI was still calculated and made available to the public for quick reference at the NOAA/National Environmental Satellite, Data, and Information Service (NESDIS)/Office of Satellite Data Processing and Distribution (OSDPD) (see http://www.osdpd.noaa.gov/PSB/IMAGES/gvi.html). We call the NDVI calculated in this manner the "raw NDVI" given it is derived directly from the weekly composited raw channel 1 and channel 2 counts within the GVI system. It is worthwhile to point out that such raw NDVI meets the demand in data availability right after the weekly composite and has a wide range of practical applications in assisting real-time monitoring of vegetation status, drought, water resources, and agriculture food production worldwide. It is especially valuable to regions that are poor in ground-based observation networks, such as Africa, etc., and it opens the opportunities for further investigations to process and reprocess AVHRR-based vegetation indices with more robust algorithms addressing different sources of error.

[10] In this study, we will not directly use the raw NDVI from GVI. Instead, we use the GVI weekly AVHRR channel 1 (VIS) and channel 2 (NIR) composites (i.e., channel counts) as inputs for further processing.

3. Methodology

3.1. Procedure to Derive Quality-Improved NDVI From GVI Outputs

[11] While operational difficulties persist with producing real-time (defined here as weekly) vegetation products, where errors are caused by the characteristics of the AVHRR instrument and by the intrinsic nature of rapid updates via land remote sensing, post launch calibration was developed to correct the time degradation of AVHRR sensors and partially the orbit drifting of the polar-orbiting satellites [*Rao and Chen*, 1995]. There are various and sound post launch calibrations for AVHRR VIS and NIR channels. We follow NESDIS/Center for Satellite Applications and Research (STAR) calibration team's development and update (including *Rao and Chen* [1995]), which is an established ongoing process. This made it possible to recalculate NDVI using post launch-calibrated AVHRR VIS and NIR reflectances converted from the GVI weekly channel counts (whereas such channel count-to-reflectance conversion and reflectance post launch calibration were not part of the GVI system itself). Such recalculated weekly NDVI has improved data quality. However, accurate post launch calibration cannot completely remove or reduce the noise in NDVI due to cloud contamination. It is further significant that a multistep mathematical smoothing method was developed and applied to the recalculated weekly NDVI (from the post launch-calibrated AVHRR NIR and VIS channel reflectances) time series to reduce the impact of persistent cloud and other artifacts [*Kogan*, 1990]. This filtering technique has been tested for a variety of downstream uses of NDVI [*Kogan*, 1990, 1997, 2001]. *Seiler et al.* [2000] have demonstrated that the applied method to minimize the artifacts helped to produce NDVI, which matched well with ground observations of vegetation and environmental phenomena. We call the resulting filtered NDVI the "smoothed NDVI. " It greatly reduced the impact of cloud and short-term weather fluctuation on vegetation. However, over the long term, the smoothed NDVI time series still exhibits a moderate to large anomalous trend, especially due to discrepancies among different AVHRR sensors onboard earlier and later NOAA satellites [*Jiang et al.*, 2008].

[12] A mathematical/statistical method has been applied to implicitly address the lumped effect of most of the instrument-related trends from NDVI based on a correction to all smoothed NDVI using the adjusted cumulative distribution

function (ACDF) (derived from a benchmark AVHRR NDVI climatology based on the best AVHRR instrument performance years) [*Jiang et al.*, 2008]. Such an adjustment has stabilized the long-term global NDVI time series. The raw AVHRR data contributing to the ACDF-adjusted global NDVI weekly time series include those from NOAA-7 (week 35 of 1981 to week 15 of 1985), NOAA-9 (week 15 of 1985 to week 44 of 1988 and week 37 of 1994 to week 6 of 1995 when NOAA-11 data were not reliable), NOAA-11 (week 45 of 1988 to week 36 of 1994), NOAA-14 (week 7 of 1995 to week 52 of 2000), NOAA-16 (week 1 of 2001 to week 11 of 2004), NOAA-17 (week 12 of 2004 to week 34 of 2005), and NOAA-18 (after week 34 of 2005) satellites. The algorithm for NDVI adjustment, given its simplicity, meets the "initial production" requirement by the NWP community.

3.2. Deriving GVF From NDVI

[13] NDVI has been well established in the literature as the key remote sensing land surface vegetation parameter for a wide range of applications. It is calculated as $\mathrm{NDVI} = (\rho_{\mathrm{NIR}} - \rho_{\mathrm{VIS}})/(\rho_{\mathrm{NIR}} + \rho_{\mathrm{VIS}})$, where ρ_{VIS} is the remotely sensed surface reflectance in VIS band in the red portion of the spectrum where chlorophyll absorbs maximally and ρ_{NIR} is the reflectance in NIR band where light reflectance from the plant canopy is dominant. For AVHRR, these are channel 1 (VIS band 0.58–0.68 μm) and channel 2 (NIR band 0.72–1.1 μm). NDVI measures the greenness and vigor of vegetation [*Tarpley et al.*, 1984] and correlates with the fraction of photosynthetically active radiation absorbed by vegetation [*Myneni et al.*, 1997]. NDVI itself is a proxy for surface vegetation greenness.

[14] Considering from a simple and practical perspective, it is certainly reasonable and feasible to use a scaled or transformed index based on NDVI to represent the green vegetation fraction in a remote sensing land surface image pixel. For example, *Carlson and Ripley* [1997] calculated vegetation fraction as $\mathrm{Fr} = [(\mathrm{NDVI} - \mathrm{NDVI}_{\mathrm{min}})/(\mathrm{NDVI}_{\mathrm{max}} - \mathrm{NDVI}_{\mathrm{min}})]^2$, where $\mathrm{NDVI}_{\mathrm{min}}$ and $\mathrm{NDVI}_{\mathrm{max}}$ represent the minimum and maximum NDVI characterizing bare soil and fully vegetated surfaces at the sensor resolution, respectively. The second-order scaling from NDVI to Fr follows the general framework by *Choudhury et al.* [1994], and it is an indication of the nonlinear relationship between NDVI and Fr, while other researchers [e.g., *Gutman and Ignatov*, 1998] found the linear relationship between NDVI and Fr to be adequate.

[15] [*Zeng et al.* 2000] derived the fractional vegetation cover (FVC) as

$$\mathrm{FVC} = (\mathrm{NDVI}_{\mathrm{p,max}} - \mathrm{NDVI}_{\mathrm{s}})/(\mathrm{NDVI}_{\mathrm{c,v}} - \mathrm{NDVI}_{\mathrm{s}}), \quad (1)$$

where $\mathrm{NDVI}_{\mathrm{p,max}}$ is the annual maximum NDVI at a pixel, $\mathrm{NDVI}_{\mathrm{c,v}}$ is the NDVI value for each International Geosphere-Biosphere Program (IGBP) category land cover classification [*Belward*, 1996] corresponding to 100% vegetation cover, and $\mathrm{NDVI}_{\mathrm{s}}$ is NDVI value for bare soil. In practice, the determination of $\mathrm{NDVI}_{\mathrm{c,v}}$ and $\mathrm{NDVI}_{\mathrm{s}}$ requires the computation of the histogram of $\mathrm{NDVI}_{\mathrm{p,max}}$ for each IGBP category, and a certain percentile for the category can be taken empirically as $\mathrm{NDVI}_{\mathrm{c,v}}$ and $\mathrm{NDVI}_{\mathrm{s}}$. These parameters are land surface type dependent (instead of being global constants) and need to be derived separately prior to the FVC calculation. *Zeng et al.* [2003] developed a global 8 km FVC data set for 1982–2000 by this approach using the NOAA-NASA land Pathfinder NDVI data. *Miller et al.* [2006] demonstrated the sensitivity of surface energy and water balance of the NCEP Noah LSM to the MODIS vegetation fraction data set derived using this approach and found that the greatest impact on the surface energy and water balance was in summer.

[16] To clarify the physical meaning of GVF used in this study, it is worthwhile to discuss the differences among the notions of different vegetation indices and their implications. NDVI is a widely accepted remote sensing land surface greenness parameter, and it is the basis for other vegetation indices such as vegetation fraction and leaf area index (LAI). Fractional vegetation cover is the fraction of vegetated area within a remote sensing land surface pixel. It has been discussed in depth by *Zeng et al.* [2000], justifying that FVC (in the way it was defined in their study) is a representation of the horizontal coverage of vegetation within a remote sensing image pixel, and it is pixel and land type dependent but not seasonal dependent, while LAI is a representation of the vertical density of vegetation within an image pixel. In other words, as season changes within an annual cycle, FVC is a constant quantity. Their approach argued that, while FVC is a fixed quantity, the within-annual seasonal change of vegetation for a pixel should be reflected in LAI. On the other hand, they also pointed out that assuming fixed LAI and seasonally varying green vegetation fraction for a pixel is an alternative treatment and a valid approach, which was the method by *Gutman and Ignatov* [1998]. Given the previous endeavors in the literature, users are cautioned to have the limitations in mind that it is difficult, if not impossible, to distinguish horizontally dense, vertically sparse vegetation from vertically thick, horizontally sparse vegetation from space just based on NDVI.

[17] In this study, considering the real-time production needs at the operational NOAA agency, we use the notion of green vegetation fraction (GVF) following *Gutman and Ignatov*'s [1998] definition. In particular, we consider the following from both theoretical and practical perspectives in developing the GVF that can be used by a wide range of numerical models: (1) GVF is different from FVC. The former is a description of how "green" a land pixel is when seen from space. It has the underlying assumption that the "green" portion of the land pixel has the uniform LAI, meaning that the evapotransipiration is not limited by LAI on the green portion within a pixel. The latter just tells the fraction of the pixel that is occupied by vegetation, regardless whether such vegetation is green (e.g., full growth) or not green (e.g., partial growth or dormant), while the underlying assumption is that the "greenness" part is reflected by another parameter, LAI. It appears that *Miller et al.* [2006] used these two definitions interchangeably by using the product derived from equation (1) but naming the parameter as "green vegetation fraction" instead of "fractional vegetation cover." (2) FVC is not directly linked to the real-time satellite-observed surface greenness or NDVI, but rather it is linked to the annual statistical properties of NDVI within a predefined land category. FVC itself is not a real-time updated parameter, thus lacking real-time monitoring capability. It is derived after a full annual cycle of NDVI data is collected. (3) Intuitively, a spaceborne remote sensor (such as AVHRR) does not need a prior knowledge of land surface type or land cover category in order to tell which part of the surface is green and which is

not. Therefore, from a data interdependency point of view, it may be cumbersome to require the prior knowledge of land surface type information (which were derived at least partially from remotely sensed surface vegetation index) in order to derive vegetation fraction. (4) Given the lack of real-time information in FVC, it cannot detect or capture real-time vegetation changes within an annual cycle, such as deforestation, desertification, and land cover/land use changes, while it can still detect changes across different annual cycles. FVC is useful in monitoring interannual and long-term changes of global vegetation. It may or may not be useful for real-time numerical land surface models, depending on how the model parameterizations are treating vegetation fraction and LAI. In particular, for the Noah LSM, it uses GVF not FVC.

[18] These considerations justify deriving weekly updated GVF from real-time satellite observations. To take advantage of the real-time signals reflected in weekly NDVI, we follow the general approach by *Gutman and Ignatov* [1998]. Not only does it directly relate to real-time observed NDVI from space, but also it has the simple formulation that will enable less distortion to the real-time signal in NDVI and requires significantly fewer parameters than equation (1). Namely, GVI is calculated following *Gutman and Ignatov* [1998] as

$$\mathrm{GVF} = (\mathrm{NDVI} - \mathrm{NDVI}_0)/(\mathrm{NDVI}_\infty - \mathrm{NDVI}_0), \qquad (2)$$

where NDVI_0 is the minimum NDVI for bare soil and NDVI_∞ is the maximum NDVI for dense vegetation. Both were global constants from the AVHRR sensor at the specific resolution in this study, independent of vegetation and soil type. On the other hand, NDVI_0 and NDVI_∞ can be sensor and spatial resolution dependent since different spaceborne sensors' detectable ranges of NDVI can be different [*Carlson et al.*, 1990]. We adopt this general framework (equation (2)) to (1) avoid dependency on other hard-to-acquire data sources for NDVI corrections in a real-time operational environment and (2) avoid data dependency on climatology or land surface type classification information, which may be inconsistent from different sources and may be updated independently from time to time. Equation (2) allows pixel-level GVF to reach its theoretical maximum (i.e., GVF = 1.0) for any land surface type or class as long as the remotely detected NDVI reaches or exceeds NDVI_∞. On the basis of analyses of the large set of data, it has been empirically determined $\mathrm{NDVI}_0 = 0.05$ and $\mathrm{NDVI}_\infty = 0.49$, taken as the 5th and 95th percentiles, respectively, from the probability distribution function of the ACDF-adjusted global weekly NDVI maps. These two parameters serve as the global bounds to ensure that the derived GVFs vary between 0.0 and 1.0, i.e., GVF = 1.0 when NDVI > 0.49 and GVF = 0.0 when NDVI < 0.05 in equation (2).

[19] For operational weekly delivery of GVF, the Global Vegetation Processing System (GVPS) has been implemented recently at NESDIS/STAR (development version) and NESDIS/OSDPD (operational version) [*Guo and Jiang*, 2008]. The GVPS uses the GVI data stream (i.e., weekly composited channel 1 and channel 2 counts) as input and generates the final GVF product in the following sequence: (1) channel count-to-reflectance conversion, post launch calibration, and NDVI calculation; (2) temporal filtering to NDVI time series following *Kogan* [1990]; (3) ACDF adjustment to smoothed NDVI following *Jiang et al.* [2008]; and (4) GVF calculation following equation (2). As a result, GVPS achieved an overall better product (e.g., smoothed and ACDF-adjusted NDVI as by-product and GVF as final product) quality than that of the GVI (e.g., raw NDVI). It provides the numerically usable weekly GVF for NWP models for the entire AVHRR operational period from late 1981 to present. GVPS mapped GVF into the GVI grid (which is a two-dimensional array of 2500 west-to-east by 904 north-to-south, covering 75°N–55°S at 0.144° pixel resolution). Then the GVI grid is mapped into the whole global array (with dimension 2500 west-to-east by 1250 north-to-south, covering 90°S–90°N) in which regions poleward of 55°S–75°N were filled by land-sea masks with a flag value denoting landmass with zero GVF.

[20] As a summary, Figure 1 shows the GVPS data flow to derive real-time weekly GVF starting from taking GVI outputs as inputs.

3.3. Filling in GVF for the Northern Hemisphere Winter Weeks

[21] For the high-latitude area (i.e., latitude > 60°N) during weeks 37–52 and weeks 1–15 (September to April, which is the Northern Hemisphere (NH) winter in high-latitude zones), there is no reliable data from the AVHRR sensor onboard polar-orbiting satellites due to the lack of sunlight during the NH late fall–winter–early spring. For the pixels in this region, GVF was assigned value 0.0 for the weeks 47–52 and weeks 1–5, then linear interpolation of time series was applied for weeks 37–46 (using GVF values at weeks 36 and 47) and weeks 6–15 (using GVF values at weeks 5 and 16). The purpose of this interpolation is to satisfy NCEP/EMC Global Forecasting System's (GFS) operational needs with minimal additional assumptions when observations are not available. Other analyses (not shown here) were performed to investigate how far south the assumption of zero wintertime GVF in weeks 47–5 should apply, but so far, the results are not conclusive. Therefore, we expect such a simple treatment to incur some artifacts in the GVF time series for pixels in NH high latitudes, while in practice, LSMs in operational NWP models have other controlling parameters that can minimize the impact of vegetation in winter in these regions where snow/ice cover and frozen soil are dominant.

4. Results

4.1. Comparison of 5 Year Monthly and 24 Year Weekly GVF Climatologies

[22] *Gutman and Ignatov* [1998] used equation (2) with $\mathrm{NDVI}_0 = 0.04$ and $\mathrm{NDVI}_\infty = 0.52$ and derived the 5 year GVF climatology from NDVI (calculated from post launch-calibrated AVHRR reflectances and spatially smoothed; see section 1, not the same NDVI as processed in this study). The above set of NDVI_0 and NDVI_∞ is different from what we used in this study. Part of the reason is that the time series filtering [*Kogan*, 1990] of NDVI has removed both the maximum and minimum values of NDVI (within the time series), while *Gutman and Ignatov* [1998] has retained all the maximum values of NDVI without applying a time series filtering when deriving monthly NDVI from weekly data. For comparison in this study, we selected the GVPS generated weekly GVF data from 1982 to 2005 and derived a climatology covering 24 years and cast in weekly intervals, which

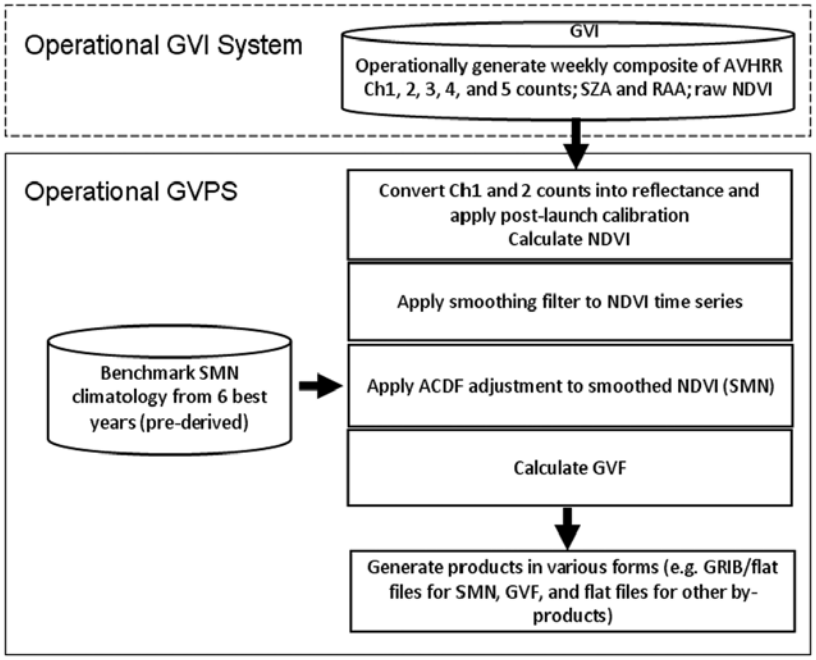

Figure 1. Global vegetation processing system (GVPS) data flow to derive GVF.

span the operational periods of NOAA-7, NOAA-9, NOAA-11, NOAA-14, NOAA-16, and part of NOAA-17 satellites. Here we denote the 5 year mean monthly GVF data set by *Gutman and Ignatov* [1998] as the "old climatology" and the newly derived 24 year mean weekly GVF data set as the "new climatology" and use these notions for brevity in the following discussion.

[23] There are qualitative differences between the new climatology and the old climatology. The first is the temporal resolution; the new climatology has 52 weekly data sets for the annual cycle, while the old climatology only has 12 monthly data sets. The second is the statistical significance; the new climatology used a much larger set of sample data than the old. The third is the data process used in deriving NDVI; the new climatology was resulted from temporally smoothed and ACDF-adjusted NDVI, while the old climatology was from the spatially smoothed and monthly averaged NDVI. The full 0.144° resolution of the operational GVI product is retained in the new climatology due to there being no spatial smoothing. The fourth is the differences in NDVI bounding values in equation (2); the new climatology was derived with $NDVI_0 = 0.05$ and $NDVI_\infty = 0.49$, and the old climatology was derived with $NDVI_0 = 0.04$ and $NDVI_\infty = 0.52$. The smaller value of $(NDVI_\infty - NDVI_0)$ in equation (2) yields a higher GVF value for a given NDVI.

[24] Table 1 shows the general qualitative differences between the new GVF data set (which includes the new GVF climatology) and the old GVF climatology.

[25] Figure 2 shows the comparison of annual cycles of the new and old climatologies for NH and Southern Hemisphere (SH), respectively. The number of land pixels (denoted as "*N*") is much larger in NH than in SH. Obviously the new climatology is generally higher than the old in both hemispheres due to the differences in derivation procedures. Figure 2a shows that the old climatology has the lowest NH GVF mean value in February, and both February and March means are lower than that of January (see the pink line in Figure 2a). This is counterintuitive, since the NH solar angle reaches the lowest during a year in December to January. Most likely, the problem is caused by the false vegetation signals due to very low solar zenith angles in the NH high-latitude winter weeks as described in section 3.2. The new climatology gets rid of this problem, presenting a reasonable transition in winter weeks with minimal NH mean GVF occurring from week 52 (end of December) to week 8 (end of February).

[26] Figures 3a–3j show the differences between the two GVF climatologies in various land types for NH. This land type classification is used operationally in the NCEP global NWP models (also depicted by *Jiang et al.* [2008, Figure 4, and reference therein]), which has 13 land cover types as denoted in Figures 3a–3j. Similar to the work of *Jiang et al.* [2008] and for brevity, we excluded Class 13 (Glacial) from the analysis, combined Class 7 (Short Groundcover) and Class 12 (Cropland) into a single class, and combined Class 8 (Broadleaf Shrubs With Perennial Groundcover) and Class 9 (Broadleaf Shrubs With Bare Soil) into another single class given the similar prescription of other land surface parameters for these classes. We see minor differences for Tropical Forest (Figure 3a); moderate differences for Boreal Forest (Figure 3d), Needleleaf Deciduous Trees (Figure 3e), and Tundra (Figure 3i) in growing season; and much larger differences for Broad Leaf Deciduous Trees (Figure 3b), Broadleaf and Needleleaf Trees (Figure 3c), Broadleaf Trees With Ground Cover (Figure 3f), Short Groundcover and Cropland (Figure 3g), Broadleaf Shrubs With Perennial Ground Cover or Bare Soil (Figure 3h), Tundra (Figure 3i), and Bare Soil (Figure 3j).

[27] Generally, the new climatology is higher than the old for all classes except Tropical Forest and Tundra. It appears

Table 1. Qualitative Comparison Between the New GVF Data Set and the Old GVF Climatology

	New GVF Data Set	Old GVF Climatology
Data source	VIS and NIR channels from AVHRR onboard NOAA-7, NOAA-9, NOAA-11, NOAA-14, NOAA-16, and NOAA-17	VIS and NIR channels from AVHRR onboard NOAA-9 and NOAA-11
Spatial resolution	0.144°	0.144°
Temporal resolution	Weekly	Monthly
Data processing	Post launch calibration to VIS and NIR reflectance [*Rao and Chen*, 1995] NDVI calculated by NDVI = $(\rho_{NIR} - \rho_{VIS})/(\rho_{NIR} + \rho_{VIS})$ 15 week smoothing filter applied to weekly NDVI time series [*Kogan*, 1990] ACDF adjustment to smoothed NDVI [*Jiang et al.*, 2008] Deriving GVF from NDVI using equation (2) with $NDVI_0 = 0.05$ and $NDVI_\infty = 0.49$	Post launch calibration to VIS and NIR reflectance [*Rao and Chen*, 1995] -NDVI calculated by NDVI = $(\rho_{NIR} - \rho_{VIS})/(\rho_{NIR} + \rho_{VIS})$ Monthly composite based on weekly NDVI data, cloud screening, and spatial smoothing with 3 × 3 pixels filter [*Gutman et al.*, 1994] Deriving GVF from NDVI using equation (2) with $NDVI_0 = 0.04$ and $NDVI_\infty = 0.52$
Others	Contains both real-time updated weekly GVF and 24 year GVF climatology Real-time data produced weekly, currently operational with NOAA-19 data as inputs	Contains only 5 year mean monthly GVF climatology No further development

there are unrealistically high values from the old climatology in winter months for Needleleaf Deciduous Trees (see Figure 3e) and Tundra (Figure 3i), while the new climatology has close to zero GVF for winter weeks (e.g., weeks 1–10 and 43–52). By closely examining the land surface vegetation type map, Needleleaf Deciduous Trees (Class 5) and Tundra (Class 10) have a large number of pixels in the high northern latitudes, which are prone to AVHRR sensor artifacts in winter weeks (see section 3.2). In addition, Boreal Forest (Needleleaf Evergreen Trees) (see Figure 3d) appears to have too strong a seasonal variation compared to the Broadleaf Deciduous Trees (see Figure 3b); while intuitively it is reasonable to expect less within-annual variation for the needleleaf evergreen trees. Physical explanation for this is linked to what NDVI fundamentally represents, that is, the "vigor" of surface vegetation, which further relates to the magnitude of photosynthesis and the transpiration/evaporation. Bacause of low solar radiation and cold air and surface temperature as well as frozen soil moisture, the plant processes contributing to vegetation vigor are quite inactive, causing the low NDVI values for needleleaf evergreen trees (which are mostly located in high latitudes of NH). Another reason is the snow cover over the top of boreal forest in winter, which makes the satellite-detected vegetation signal low. Evidently, independently observed NDVI over NH boreal forest by MODIS also has very low values in winter (figure not shown here).

[28] Comparison for the SH (which has a much smaller number of land pixels than the NH) was performed with figures not shown for brevity. Similar to that for the NH, the new GVF climatology is higher than the old except for Tropical Forest (Class 1) in SH summer weeks.

[29] Note that the 0.144° resolution surface vegetation type classification map was derived from the 1° × 1° coarse resolution 13-type classification, thus characteristics seen in these class-averaged analyses are caused partly by misclassifications (when scaling from coarse to fine grid resolution).

[30] Table 2 summarizes the averaged annual GVF from the new and old climatologies as well as their differences for all classes together and for each land type in each hemisphere. It shows that the new climatology is 0.039 and 0.060 higher than the old in NH and SH, respectively. In NH, the biggest difference (valued at 0.082) is in Broadleaf Deciduous Trees and the smallest absolute difference (valued at 0.001) is in Tropical Forest and Needleleaf Deciduous Trees. In SH, the biggest difference (valued at 0.107) is in Tundra and the smallest absolute difference (valued at 0.021) is in Tropical Forest. Additionally, the differences between the new

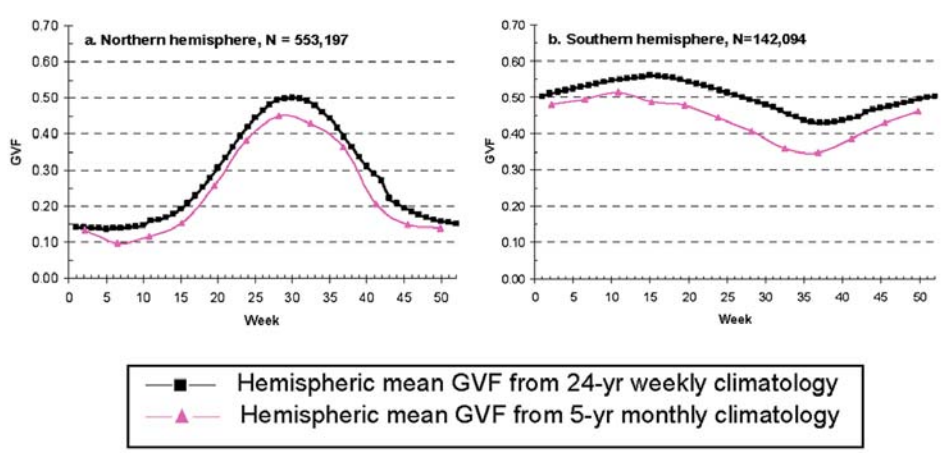

Figure 2. Annual cycles of hemispherical mean GVF from the 24 year weekly climatology and the 5 year monthly climatology: (a) Northern Hemisphere and (b) Southern Hemisphere.

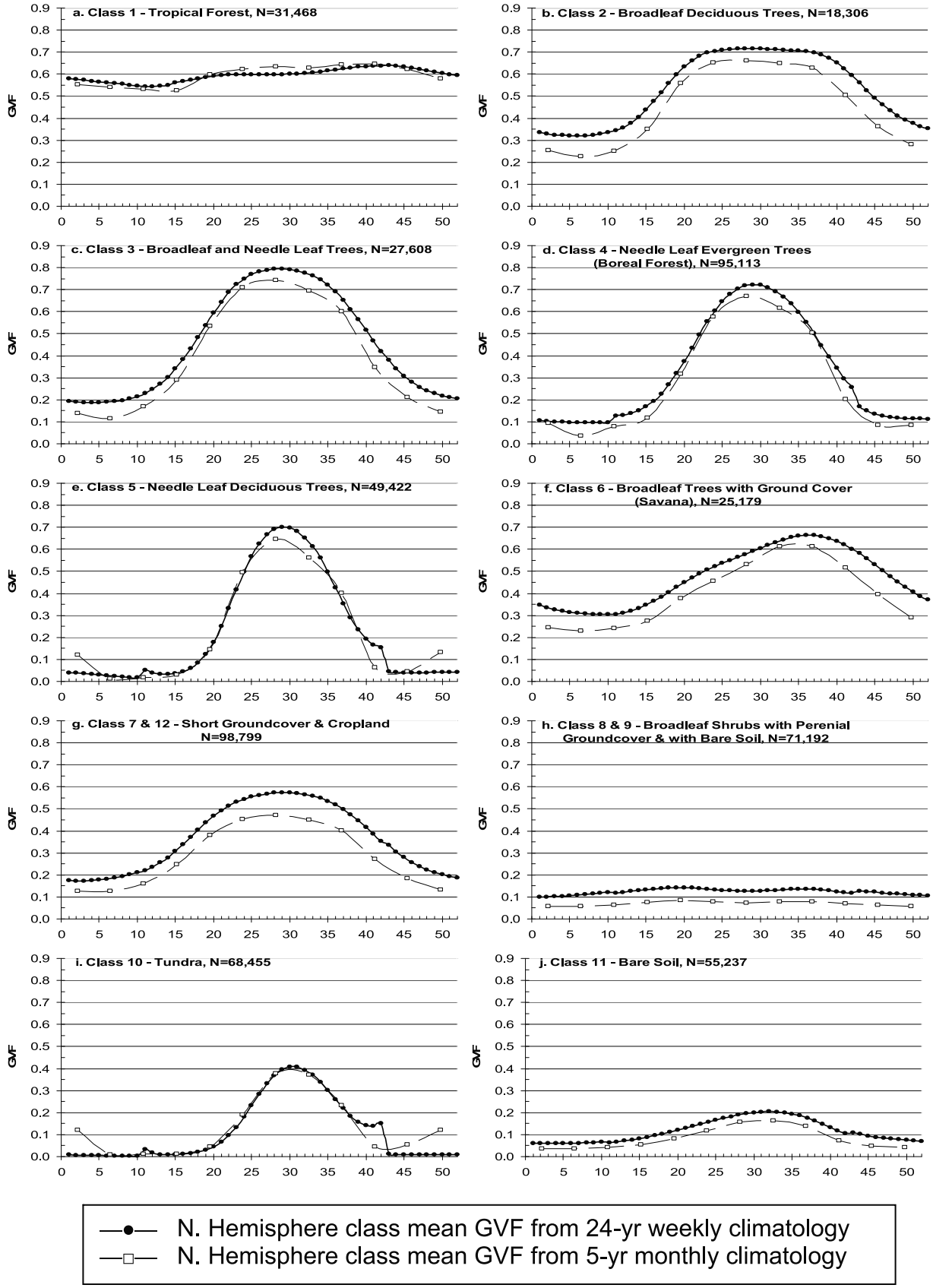

Figure 3. Annual cycles of class mean GVF from the 24 year weekly climatology and the 5 year monthly climatology for the Northern Hemisphere.

Table 2. Quantitative Differences Between the New and Old GVF Climatologies

Land Type, Class Number and Name	Northern Hemisphere			Southern Hemisphere		
	Average GVF From New Climatology	Average GVF From Old Climatology	Difference (New - Old)	Average GVF From New Climatology	Average GVF From Old Climatology	Difference (New - Old)
All Land Type Classes	0.278	0.239	0.039	0.500	0.440	0.060
1. Tropical Forest	0.594	0.593	0.001	0.688	0.709	−0.021
2. Broadleaf Deciduous Trees	0.530	0.448	0.082	0.525	0.454	0.071
3. Broadleaf and Needleleaf Trees	0.455	0.391	0.064	0.596	0.558	0.038
4. Needleleaf Evergreen Trees	0.322	0.282	0.040	0.446	0.396	0.050
5. Needleleaf Deciduous Trees	0.224	0.223	0.001	0.324	0.291	0.033
6. Broadleaf Trees With Ground Cover	0.474	0.399	0.075	0.572	0.491	0.081
7 & 12. Short Groundcover or Cropland	0.365	0.284	0.081	0.484	0.394	0.090
8 & 9. Broadleaf Shrubs With Perennial Groundcover or With Bare Soil	0.124	0.070	0.054	0.297	0.209	0.088
10. Tundra	0.113	0.133	−0.019	0.270	0.163	0.107
11. Bare Soil	0.117	0.083	0.034	0.161	0.090	0.071

climatology and the old vary on weekly and monthly time scales as shown in Figure 3.

[31] To further compare the annual cycles of the new and old GVF climatologies at a detailed level, we selected eight sites with distinctive vegetation types. The geolocations and land surface types of these sites are provided in Table 3. They include cropland, mixed forest, broadleaf deciduous trees, boreal forest (needleleaf evergreen trees), broadleaf shrubs, tundra, rainforest (tropical forest), and desert sites, as suggested by the NCEP/EMC Land-Hydrology Team. Figures 4a–4h plot the annual cycles of the new and old GVF climatologies. The GVF value at each site is an average of the 3 × 3 pixels spatial mask centered at each location. The above eight sites are selected such that within the 3 × 3 pixels the vegetation class is homogeneous. Although the general annual cycles at different sites are similar between the new and old GVF climatologies, the differences are obvious. At the Illinois (Figure 4a), Maine (Figure 4b), Ohio (Figure 4c), Sierre Madre–Occidental Mountains (Figure 4e), and Quebec (Figure 4f) sites, the new and old climatologies are closely matched for most weeks, while at the Boreas NSA site at Old Black Spruce in Canada (Figure 4d) and at South Australia (Figure 4g), the new climatology is constantly higher than the old. At the Maine site (Figure 4b), the old climatology undergoes an unusual change at the beginning of year (the abnormally low GVF in February, i.e., second month, for the old climatology), while the new climatology appears to be more reasonable. The new climatology indicates more sustained peak vegetation growth at the Illinois, Maine, and Ohio sites, which was confirmed empirically by the NCEP/EMC Land-Hydrology Team. At the boreal forest site in central Canada (Figure 4d), the new climatology is significantly higher than the old, especially in winter, which is reasonable since the site is "evergreen. " It is worth mentioning that this Boreas NSA site is one of the core sites for the EOS MODIS Land Validation System (see http://landval.gsfc.nasa.gov/coresite.php?SiteID=8). The MODIS-independent observed vegetation index (e.g., 16 day composite at 250 m) for this site from year 2000 to present indicates that its NDVI ranges approximately from 0.09 to 0.83 with very strong seasonal cycles (data available at EOS Land Validation System Web site, figure not shown here). For this site (Figure 4d), the MODIS NDVI data independently support the argument of strong seasonality for boreal forest seen here in both the new and old climatologies. Further, the above-zero minimal NDVI value (e.g., approximately 0.09 as mentioned above) from MODIS for this boreal forest site appears to indicate that the winter values of GVF from the new climatology are more reasonable than those from the old climatology (which is close to zero). At the tropical rainforest site in Para, Brazil (Figure 4h), the new climatology is much lower than the old before week 20, while after week 20, the situation reversed. Possible causes may be the explicit manual cloud removal by *Gutman et al.* [1994] for persistent cloud in tropical forest when producing the old climatology.

[32] These comparisons indicate that, overall, the new climatology is comparable to the old, with the new one having higher mean values. The new climatology provides enhanced features such as the higher spatial heterogeneity, more sustained peak vegetation growth, and more reasonable

Table 3. Selected Sites for Comparison of 24 Year Weekly GVF and 5 Year Monthly GVF Climatologies

Site	Central Location (Latitude/Longitude)	Land Type
Illinois, USA	39.456°N, 89.856°W	Cropland (Class 12)
Maine, USA	46.080°N, 68.544°W	Mixed Forest (Class 3)
Ohio, USA	40.032°N, 81.072°W	Broadleaf Deciduous Trees (Class 2)
Boreas NSA–Old Black Spruce, Canada	55.880°N, 98.481°W	Needleleaf Evergreen Trees (Class 4)
Sierre Madre–Occidental Mountains, Northwest Mexico	30.312°N, 108.070°W	Broadleaf Shrubs (Class 8)
Quebec, Canada	59.112°N, 74.810°W	Tundra (Class 10)
Rainforest, Para, Brazil	3.096°S, 55.800°W	Tropical Forest (Class 1)
Desert, South Australia	29.880°S, 135.000°E	Broadleaf Shrubs With Bare Soil (Class 9)

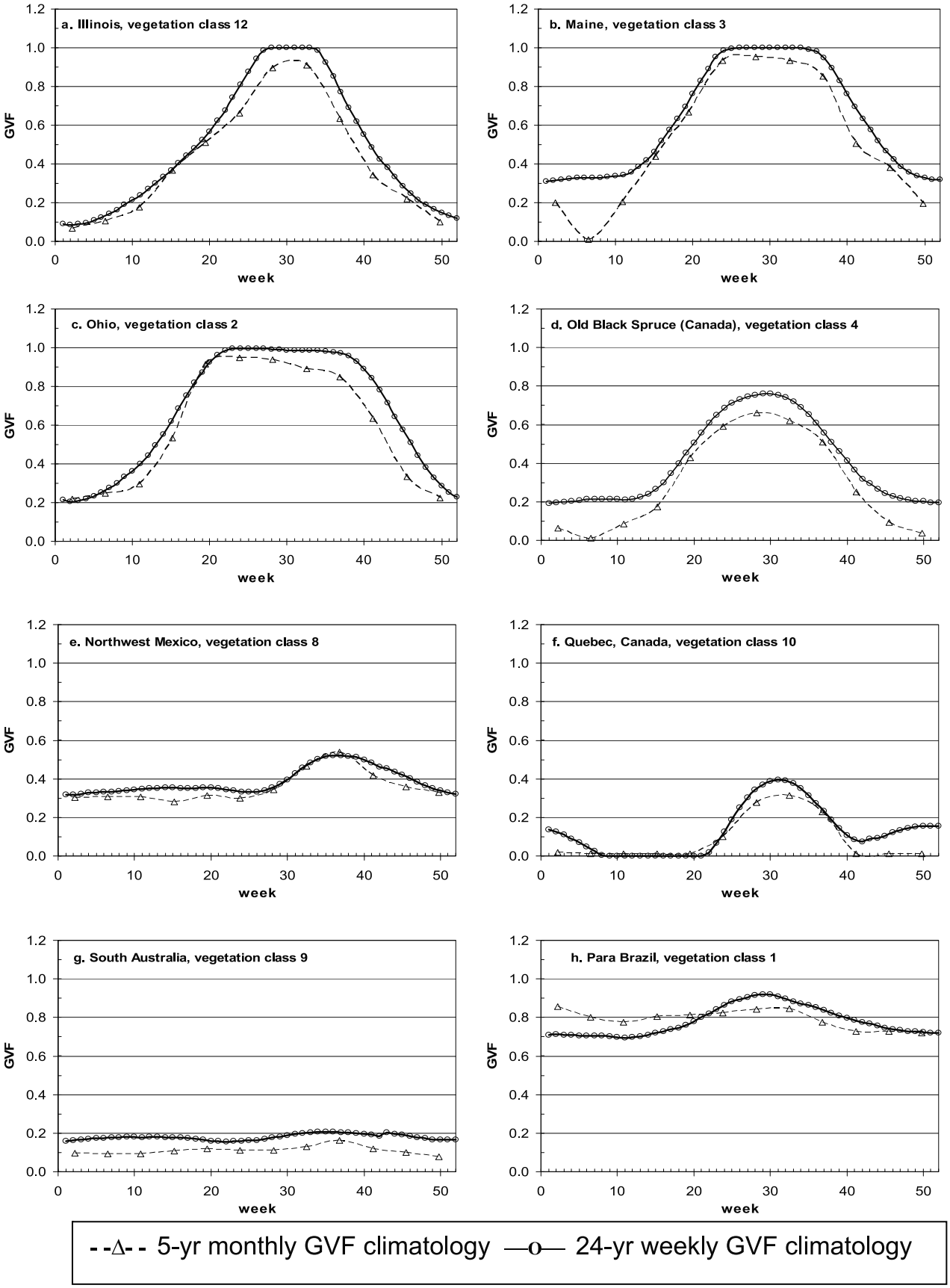

Figure 4. Annual time series of 24 year GVF climatology and 5 year weekly GVF climatology at different sites.

transitions in winter weeks for a few classes in both hemispheres.

4.2. Evaluation of the Real-Time GVF

[33] A significant advantage of the new GVF weekly data set is the real-time updated information on surface vegetation. Figures 5a–5j show the differences between real-time weekly GVF and the new GVF climatology (i.e., 24 year mean GVF, plotted as same repeating annual cycles in red line overlaid with real-time weekly GVF in black line) for each class. The difference between the two curves depicts the class-specific real-time anomalies. Reasons for these anomalies are the natural variation in vegetation growth (especially over land types in which interannual variability in vegetation growth is highly sensitive to precipitation and soil water content), severe AVHRR sensor degradation (e.g., strong negative anomalies in 1994 due to replacement of NOAA-11 by NOAA-9, which was already seriously degraded from late 1994 to early 1995; e.g. Figures 5a, 5b, 5f), sensitivity to cloud contamination (e.g., in tropical areas due to persistent cloud), and sensitivity to aerosol contamination (e.g., in 1991 for tropical areas due to Mt. Pinatubo eruption; Figures 5a, 5f, etc.), among others. Figure 5 also shows that the severe sensor degradation in 1994 affects some classes (e.g., Tropical Forest, Broadleaf Deciduous Trees, and Broadleaf Trees With Ground Cover) more than others. This is because the AVHRR VIS and NIR bands (used to derive NDVI) are more sensitive to dense vegetation-covered pixels than to mixed or bare soil dominant pixels. The impacts of volcanic ashes (in 1991) are more obvious on tropical region classes than on others, because the major propagation of ashes was within the tropics.

[34] Figures 6a–6h show real-time GVF for the eight sites selected in Table 3. The Sierre Madre-Occidental Mountains site in northwest Mexico (Figure 6e) has significant interannual variations of GVF, which is the characteristic of a semiarid climate regime where vegetation is very sensitive to regional precipitation. This site usually has a rapid spring vegetation green up, while in drought years, it may be less so. Similarly, the desert site in South Australia (Figure 6g) also has very significant interannual vegetation variation. At the Illinois site (Figure 6a), the differences between the annual vegetation conditions (and resulting GVF) and the climatology are not very significant. At the rainforest site in Para, Brazil (Figure 6h), the real-time GVF tends to be often smaller than the GVF climatology, most likely due to persistent cloud contamination in individual years.

[35] Surface vegetation anomalies are strongly related to the cumulative precipitation anomalies in a region. As part of the assessment in this study, we look at the correspondence between the 30 day and 90 day cumulative precipitation anomalies and the real-time GVF anomalies. The precipitation anomalies data are available online at http://www.emc.ncep.noaa.gov/mmb/gcp/cpcrfc/cpc3090.html. Figure 7 shows qualitatively the correspondence between real-time GVF anomalies and the 30 day (Figure 7a) and 90 day (Figure 7b) cumulative precipitation anomalies ending 31 July 2006. These anomalies indicate a severe drought occurred across the region from North Dakota, South Dakota, to Texas, which is the grain-growing zone of the CONUS. Figures 7c, 7d, and 7e show the GVF anomalies for week 26 (starting 27 June), week 27 (starting 4 July), and week 28 (starting 11 July) of 2006. Apparently the GVF anomaly patterns in these periods match the overall accumulated precipitation anomaly patterns shown in Figures 7a and 7b. Such comparison, although not to be interpreted as validation in a strict sense, provides strong justification for the real-time weekly GVF fields to be used by numerical models in order to capture the major drought signals that could alter the model responses in terms of regional surface fluxes and precipitation forecasting accuracy. In the northeast part of the CONUS (which is a nonarid region), it appears to be anomalously wet, although the GVF has a negative anomaly. The reason, among others, may be attributed to the excessive precipitation (thus excessive cloud) along with abnormally low near-surface temperature, which could create a less than optimal environmental condition for vegetation growth.

4.3. Partial Validation by Independent NDVI Observations From MODIS

[36] It remains a challenge to globally validate the new GVF data set using independent observations. One difficulty is that GVF observations at the current 0.144° grid resolution do not exist, either from ground-based, airborne, or spaceborne sensors. To provide a data quality assessment with available and independently obtained observations, we use the EOS MODIS NDVI product surrounding a few EOS land validation core sites (see http://lpvs.gsfc.nasa.gov/LPV_CS_gen.html and references therein) within the CONUS.

[37] Since the MODIS-based NDVI and the AVHRR-based GVF (derived in this study) are not equivalent, we cannot compare them directly. Instead, we compare the MODIS NDVI standardized anomalies with the AVHRR GVF standardized anomalies, where the standardized anomaly for a specific data set is defined as the "real-time value" minus the "time series mean" or "climatological mean" then divided by the "time series standard deviation." The MODIS NDVI used here is from the latest version 5 (or Collection 5) Global MOD13A2 vegetation indices, which contain the 16 day composite NDVI at 1 km resolution. The accuracy has been assessed via vigorous validation efforts, and the data are ready for use in scientific studies (see https://lpdaac.usgs.gov/lpdaac/products/modis_products_table/vegetation_indices). Before comparison, MODIS NDVI were resampled into the specific GVF grid (at 0.144° spatial resolution) covering the selected core site.

[38] In addition, another independently processed AVHRR-based NDVI data set was included for comparison. This data set was produced by the Global Inventory Modeling and Mapping Studies (GIMMS) group [*Tucker et al.*, 2005]. The GIMMS NDVI long-term data set (available at http://glcf.umiacs.umd.edu/data/gimms) is based on time series decomposition and reconstruction to remove sensor degradation related trends and has been corrected for calibration, view geometry, volcanic aerosols, and other effects [*Pinzon et al.*, 2005]. To be consistent with the above, the GIMMS NDVI standardized anomalies were calculated in the same manner as the above MODIS NDVI standardized anomalies.

[39] Four EOS land validation core sites are selected within the CONUS. These are the ARM/CART, SGP in Oklahoma centered at [36.640°N, 97.500°W], Cheq-Niolet in Wisconsin centered at [45.946°N, 90.272°W], Jornada LTER in New Mexico centered at [32.600°N, 106.860°W], and Walker Branch in Tennessee at [35.958°N, 84.287°W]. Figure 8a

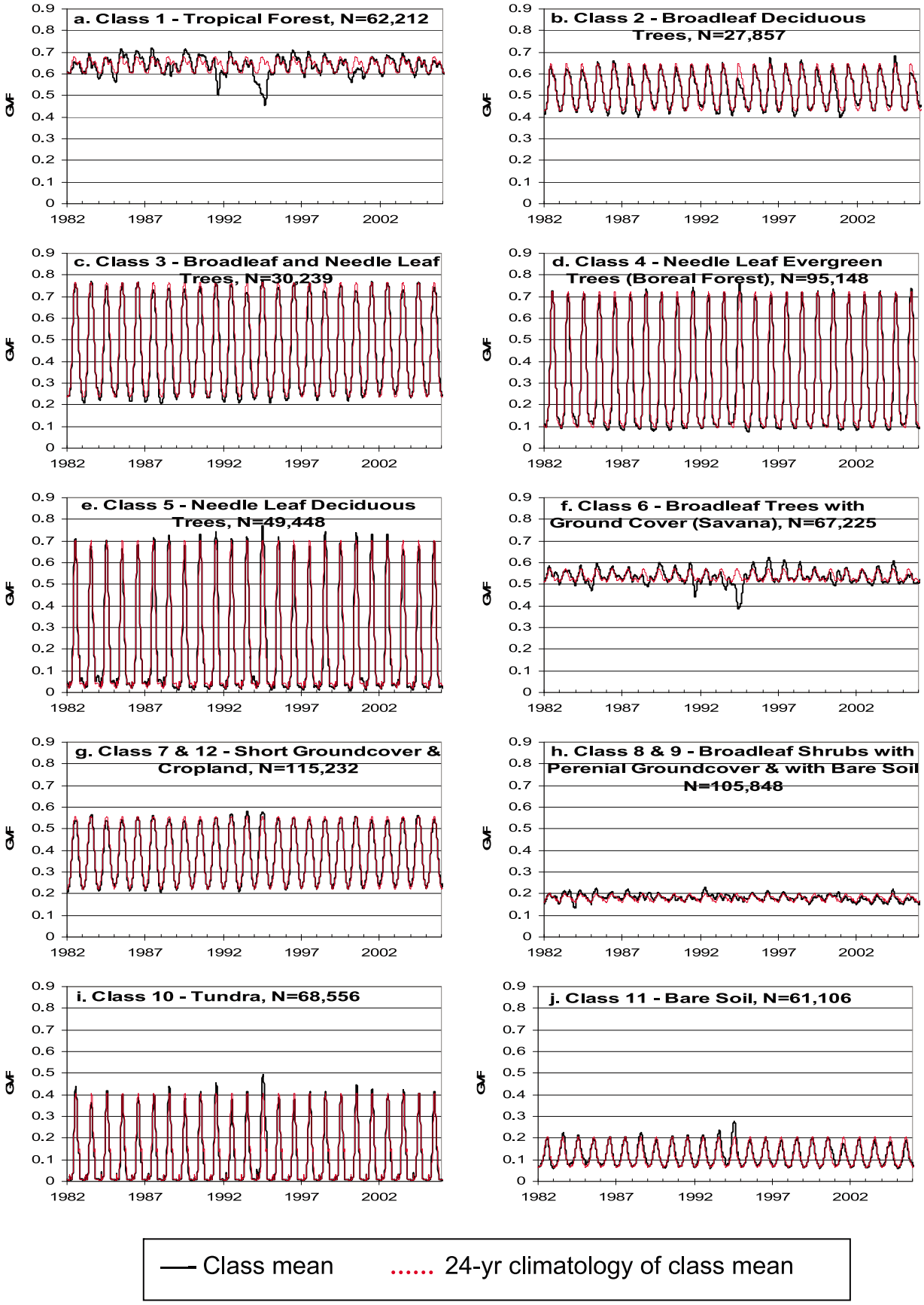

Figure 5. Multiyear time series of class mean real-time weekly GVF and weekly GVF climatology for each class.

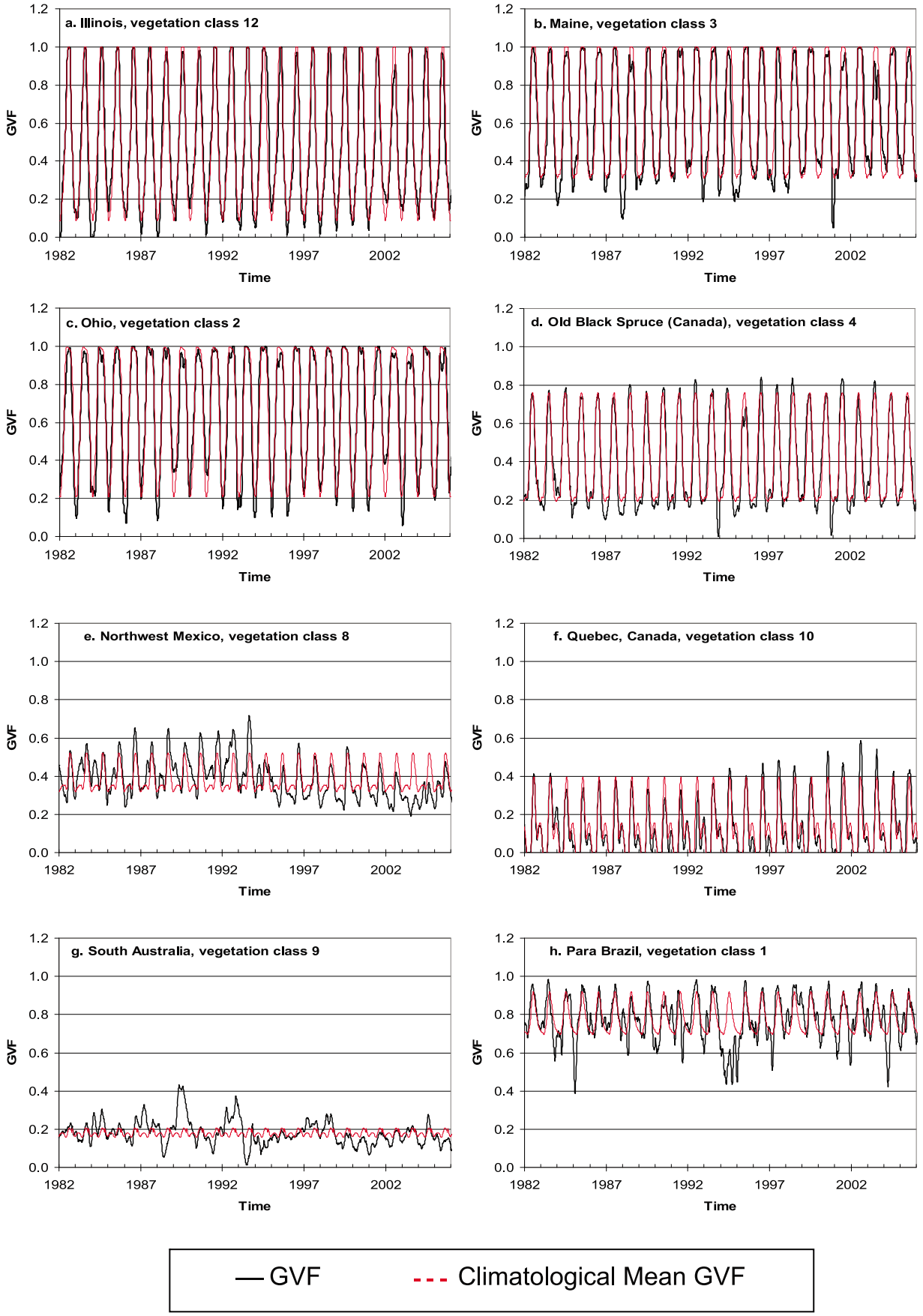

Figure 6. Comparison of real-time GVF and climatological mean GVF for different sites.

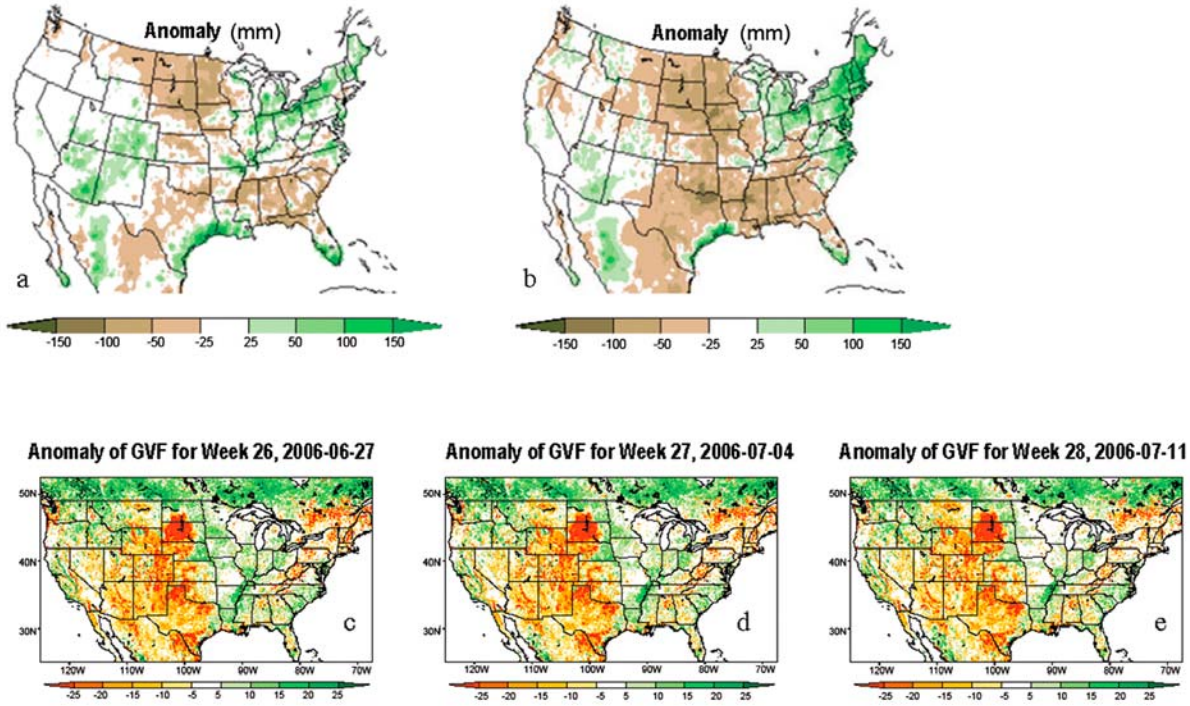

Figure 7. Accumulated precipitation anomaly (unit: mm) and weekly GVF anomaly (unit: 1/100) at CONUS: (a) 30 day accumulated precipitation anomaly ending 31 July 2006; (b) 90 day accumulated precipitation anomaly ending 31 July 2006; (c) GVF anomaly for week 26 (starting 27 June 2006); (d) GVF anomaly for week 27 (starting 4 July 2006); (e) GVF anomaly for week 28 (starting 11 July 2006).

shows the Palmer Drought Index of July 2006 (see NESDIS/National Climatic Data Center archive at http://lwf.ncdc.noaa.gov/sotc/index.php?report=drought&year=2006&month=jul) over the CONUS with locations of these core sites indicated as b, c, d, and e, respectively. This shows that in July 2006, severe to extreme droughts occurred in the western CONUS, especially in North Dakota, South Dakota, and parts of Okalahoma and Texas, and moderate to extreme droughts occurred in parts of the southeast states, while other places such as parts of Arizona, New Mexico, and northeastern states had moderate to extreme moist conditions (see Figure 8a for details). The above-selected core sites, ARM/CART (Oklahoma), Cheq-Noilet (Wisconsin), Walker Branch (Tennessee), and Jornada LTER (New Mexico), were in severe drought, midrange or normal, moderate drought, and extreme moist regions, respectively, in July 2006, according to Figure 8a.

[40] Figures 8b–8e show the time series of the standardized anomalies of GVF (from GVPS), MODIS Terra (morning overpass satellite) NDVI, MODIS Aqua (afternoon overpass satellite) NDVI, and GIMMS NDVI at the above four sites from the beginning of 2001 to the end of 2006. (Note that Terra data started earlier than Aqua, and Aqua NDVI is only partially available in 2006). The general trends as well as magnitudes (of standardized anomalies) match well among these different data sets. Compared to MODIS NDVI, the new GVF data set exhibits smoother within-annual and interannual transitions. Compared to the GIMMS NDVI, the new GVF data set is much smoother. At the ARM/CART (Oklahoma) site (Figure 8b), all appear to be able to capture the severe drought in 2006 (e.g., magnitudes of peak values of different curves in 2006 are the lowest among the displayed years). At the Cheq-Noilet (Wisconsin) site (Figure 8c), the interannual peak magnitudes are similar. The various data sets appear to differ the most at the Jornada LTER (New Mexico) site (Figure 8d) among the four. This site is an extremely moist region in July 2006 (see Figure 8a). All data sets are able to capture the strong positive vegetation anomalies for this period. For other years, MODIS Terra and Aqua have moderate differences at times, and the new GVF data set has large differences from MODIS NDVIs such as 2003 and 2004, and so does the GIMMS NDVI. At the Walker Branch (Tennessee) site (Figure 8e), the new GVF data set is consistent with the MODIS NDVIs, while the GIMMS NDVI appears to be less so. In July 2006, this site is in a moderate drought and the new GVF data set is slightly lower than previous years while this is less obvious in MODIS NDVIs and GIMMS NDVI.

[41] Although it is planned to validate the new GVF data set more comprehensively, these limited comparisons are encouraging and have demonstrated that the new data set can capture the real-time strong vegetation anomalies corresponding to droughts and moist conditions and the new GVF data set is smoother than other independent NDVI data sets, which is a desirable feature for numerical models.

4.4. New GVF Impact Study Using Operational NCEP Model

[42] The impact study is to (1) investigate whether the new GVF climatology can improve forecasts compared to the old climatology and (2) assess whether the new real-time weekly

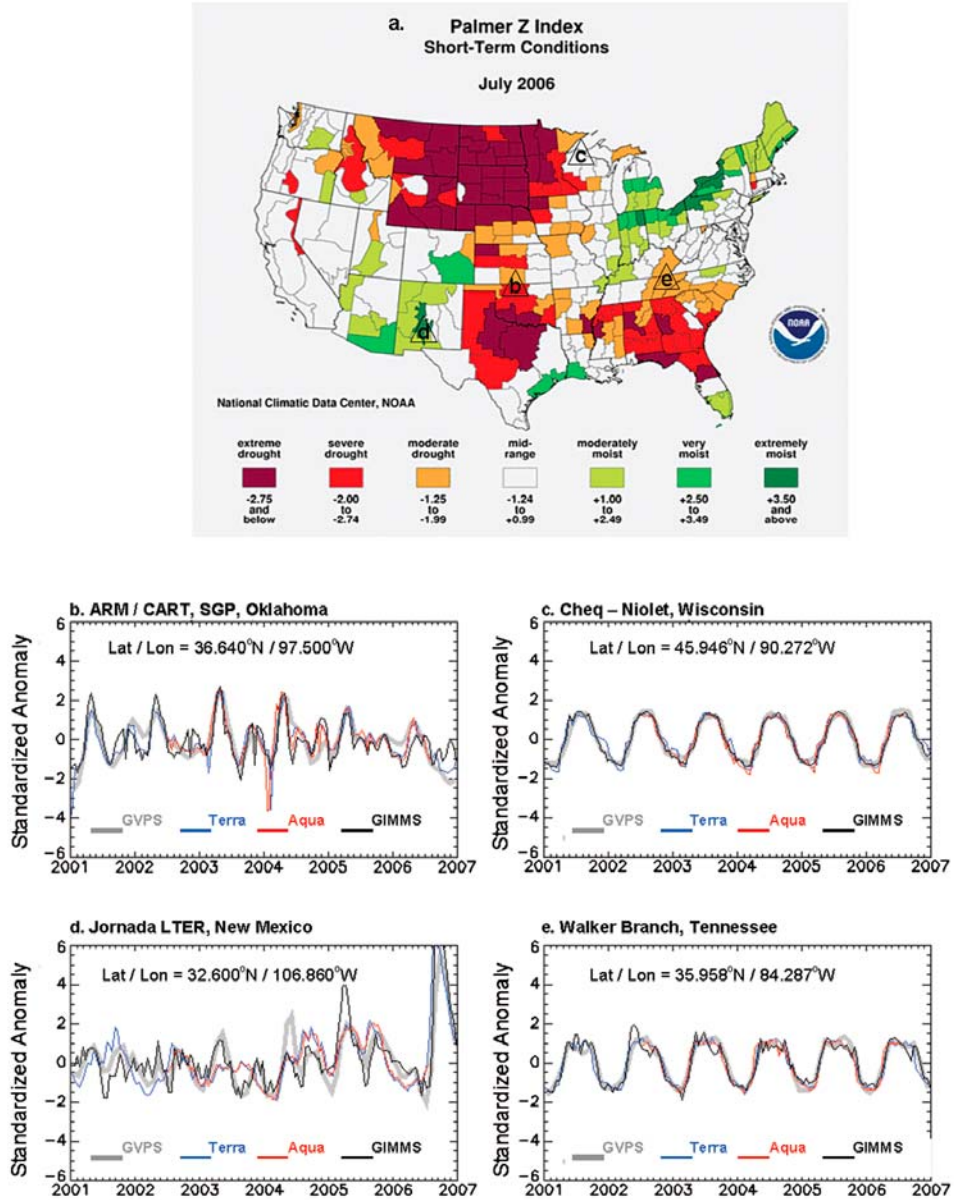

Figure 8. (a) Palmer Drought Index over CONUS for July 2006 with locations of selected EOS land validation core sites indicated as b, c, d, and e. (b) Time series of standardized anomalies from GVPS GVF (gray line), MODIS Terra (blue line), MODIS Aqua (red line), and GIMMS NDVI (black line) at the ARM/CART, SGP, Oklahoma site. (c) Similar to Figure 8b but for Cheq-Niolet, Wisconsin site. (d) Similar to Figure 8b but for the Jornada LTER, New Mexico site. (e) Similar to Figure 8b but for the Walker Branch, Tennessee site.

GVF data can improve the model predictions at the surface compared to the new GVF climatology.

[43] The tests were conducted in the NCEP Weather Research and Forecasting-Nonhydrostatic Mesoscale Model (WRF-NMM) system. The land surface module in this system is the Noah LSM, which uses the 13 vegetation types described earlier in this paper. A set of parameters for each vegetation type was created from a variety of biometric and physiological data sources. Noah LSM assumes the vegetation portion within a model grid is transpiring at its maximum rate (e.g., with a fixed LAI value set as 3.0), while only GVF is allowed to vary in time and space.

[44] The GVF data sets were spatially interpolated to the CONUS domain at 12 km resolution. A large set of model runs was conducted for 17 days from 2 to 18 July 2006. Each model run is for 84 h starting at a fixed model initialization time each day (1200 UTC); thus, 17 days have 17 model runs. These cases were categorized as the Control Run (CTRL) using the old GVF climatology, the Experimental Run 1 (EXP1) using the new GVF climatology, and the Experimental

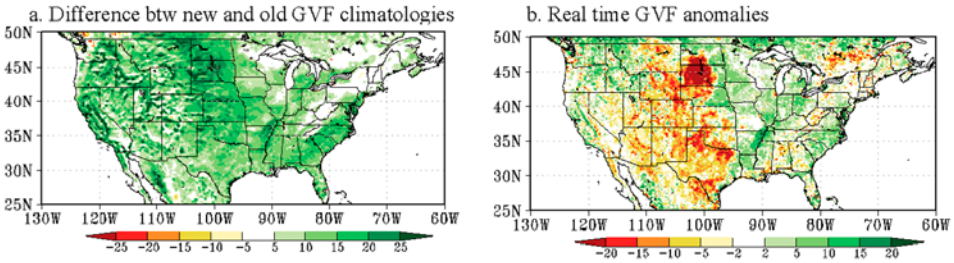

Figure 9. The averaged GVF differences for the period of 2–18 July 2006: (a) GVF differences between the new (24 year weekly) climatology and the old (5 year monthly) and (b) real-time GVF anomalies relative to the new GVF climatology (new real-time minus new climatology).

Run 2 (EXP2) using the new real-time weekly GVF. Thus, the total number of model runs is 51. The model grid, physical process schemes, and initial and boundary conditions are identical in these three cases except for the GVF specified in the surface parameter input file. Results for each case (CTRL, EXP1, or EXP2) are an average of the 17 individual 84 h simulations. Such an experiment design is robust, avoiding model simulation results being significantly biased by any individual model run.

[45] The model outputs every 3 h, starting from the 1200 UTC initialization time. The 17 averaged 84 h period results from these simulations were put into two studies (A and B). Study A represents the simulations using the new climatology minus the simulations using the old climatology, investigating the impacts of climatological GVF differences on the forecasts. Study B represents the simulations using the new real-time GVF data minus those using the new climatology, investigating the impacts of real-time GVF anomalies on the forecasts. The model results were validated against 3 h surface observations of 2 m air temperature and relative humidity using the NCEP/EMC Forecast Verification System. The biases and root mean square errors (RMSEs) for the forecasts were calculated for CONUS and individual subregions.

[46] Figure 9 shows the difference between the new GVF climatology and the old (see Figure 9a) and the real-time GVF anomalies in July 2006 (see Figure 9b) over CONUS. The new GVF climatology is higher than the old over most parts of CONUS with the largest differences of about 20% over the southeast and northern Midwest and West Coast of California. The real-time GVF is lower in the west and slightly higher in the east part of CONUS compared to the new GVF climatology. This reflects drought over many parts of the west CONUS, especially the severe drought in North Dakota, South Dakota, and part of Texas, which occurred before and during summer in 2006 (also see section 4.2).

[47] Figure 10 shows the day 2 forecast differences at 1600 U.S. Eastern Time (EST) from Study A, which is 33 h after model run. In general, the new GVF climatology cools surface temperature (Figures 10a and 10b) over most regions, with the largest cooling in areas where the new climatology increases most (compared to the old GVF) and where GVF itself is high. The latent heat (Figure 10c) and 2 m dew point temperature (Figure 10d) increases significantly over most regions, while the sensible heat (figure not shown) decreases with a smaller magnitude. These results are physically sound as more of the net radiation is dissipated in form of latent heat via enhanced evapotranspiration (evaporative cooling) in response to increased GVF.

[48] For the drought-induced decrease in GVF over west CONUS (Figure 9b), Figure 11 shows results from Study B on day 2, latent heat flux (Figure 11c) and 2 m dew point temperature (Figure 11d) decreases in response to GVF negative anomaly, as a result both surface skin temperature (Figure 11a) and 2 m temperature (Figure 11b) increases. However, the 2 m temperature increases less than the skin temperature in both magnitude and spatial extent and is mainly limited to the areas where severe drought occurred.

[49] The model predicted 2 m surface temperature and relative humidity were compared to the observations with the 17 day averaged biases (defined here as the forecast minus the observation) and RMSEs were calculated. For 2 m temperature, the biases for all simulations (Figure 12a) have a diurnal cycle with the old GVF run, showing the biggest warm biases. Such warm biases are higher during daytime and lower during late night and early morning. Both the daytime and nighttime biases were reduced when the new GVF data (either new climatology or real-time GVF) were used, especially during daytime (when the warm biases were reduced by about 0.5°C). The RMSEs for 2 m temperature in all simulations (Figure 12b) show a diurnal cycle, superimposed on an increasing trend with the forecast time with maximums at daytime. Evidently, the simulations using the new GVF data have lower RMSE than those using the old GVF climatology.

[50] For 2 m relative humidity, all simulations have negative biases at almost all forecast hours (Figure 12c), with the values of up to −7% from the simulations using the old GVF climatology. The daytime and nighttime biases are all reduced when the new GVF data were used. The RMSEs (Figure 12d) exhibit a similar diurnal cycle as the 2 m temperature, with a minimum of approximately 12–14% and a maximum of 16–18% for the simulation using the old GVF climatology. Again, the simulations using the new GVF data have lower RMSEs than those using the old GVF climatology.

[51] NCEP Forecast Verification System divides the CONUS into 14 subregions (see Figure 13a). For brevity, the results are shown for two of these subregions. Figures 13b–13e show the bias of 2 m surface air temperature and relative humidity forecasts averaged from the 17 cases for region LMV (containing 160 surface stations) and region NPL (containing 500 surface stations). Overall improvements were gained by using the new GVF data in terms of significantly reduced biases (comparing to using the old GVF climatology; see Figures 12a and 12c). The distinctions between

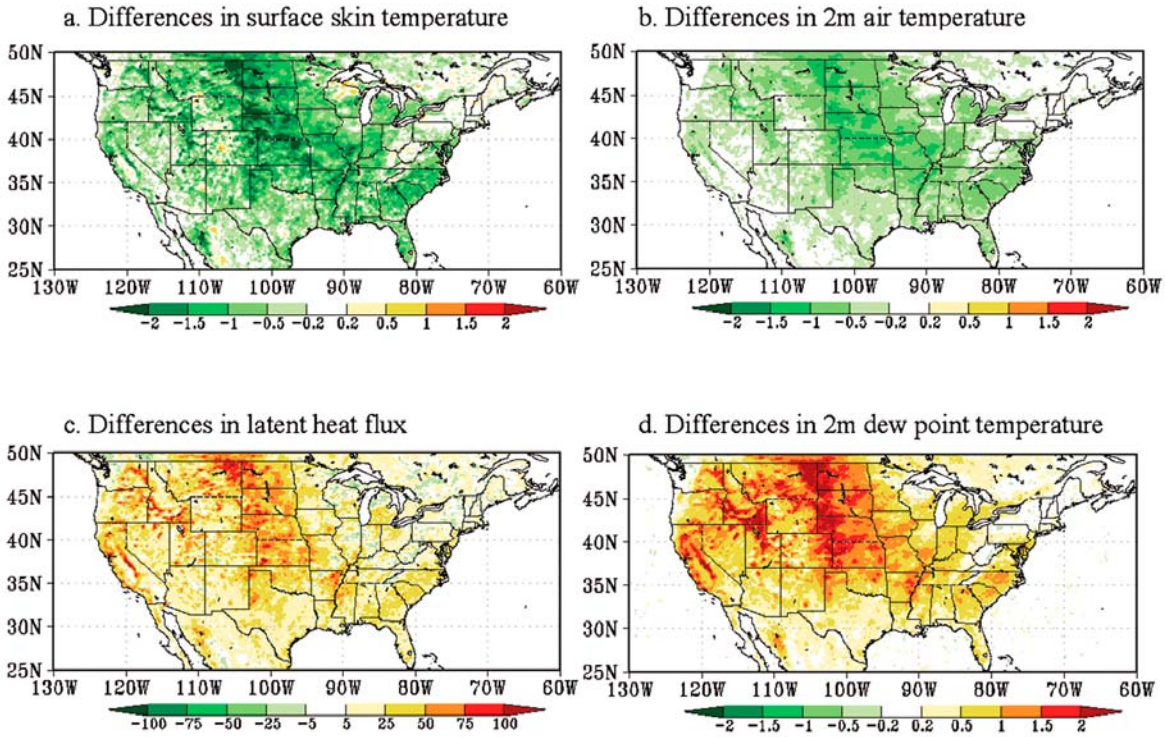

Figure 10. Surface differences (averaged from 17 model runs from 2 to 18 July 2006) by using new GVF climatology and using old GVF climatology after 33 h forecasts: (a) differences in surface skin temperature (unit: K); (b) differences in 2 m surface air temperature (unit: K); (c) differences in latent heat flux (unit: W m^{-2}); and (d) differences in 2 m dew point temperature (unit: K) (result by using the new GVF climatology minus results by using the old GVF climatology).

using the new GVF climatology and the new real-time GVF data appears to be region dependent. For example, the NPL subregion (Figures 13c and 13e) is more sensitive to the differences between the new real-time GVF and new GVF climatology, while the LMV subregion (Figures 13b and 13d) is much less so. The reason is linked to the severe drought presence in the NPL region (see Figure 9b) during the simulation period. Interestingly, the real-time GVF reduced the 2 m relative humidity biases, while it increased the 2 m air temperature biases, indicating a mixed impact to WRF-NMM performance. On the other hand, such results are physically sound and consistent with those shown in Figure 11b. That is, for the severe drought areas, real-time GVF (which is lower than the 24 year weekly GVF climatology) resulted in 2 m temperature increases (see the blue curve in Figure 13c), but such increases were not as much as that by using the old 5 year monthly GVF climatology (which caused more severe warm biases; see the red curve in Figure 13c). Another perspective is that GVF is not the only parameter that controls the model's 2 m air temperature. Figure 13c shows there is an overall warm bias in the model 2 m air temperature regardless of which GVF data used.

[52] These intensive but still limited simulations appear to indicate that the major differences in model responses are caused by the differences in the new and old GVF climatologies rather than by the weekly anomalies in the new GVF data sets, while the model sensitivity to the real-time GVF anomalies is physically sound and regional dependent. Other details of these simulations are described by *Tian et al.* [2008].

5. Discussion

[53] It is worthwhile to point out the different perspectives when generating the quality-improved land surface NDVI and GVF products in a reprocessing mode, in contrast to that in an operational mode (which is the context of this study). In a reprocessing mode, which is not time critical, physically based correction algorithms have been implemented to remove contamination sources to remotely sensed surface reflectance data (e.g., due to Rayleigh scattering, aerosol, water vapor, directional reflectance differences, etc.). For example, the effort by the Long-Term Data Record (LTDR) group [*Pedelty et al.*, 2007] among others applied the lessons learned in the MODIS data processing and used applicable correction modules to the AVHRR data stream [*Vermote et al.*, 1997]. Alternatively, physically based corrections can be combined with time series decomposition and reconstruction approach, e.g., by the GIMMS group. In such reprocessing context, AVHRR VIS and NIR reflectances from the GAC daily data would be physically corrected after the post launch calibration and before any mathematical or statistical based smoothing or filtering. In terms of providing physical traceability to error sources, only the physical based process generated long-term data records will meet the requirement of the "Climate Data Record," which requires

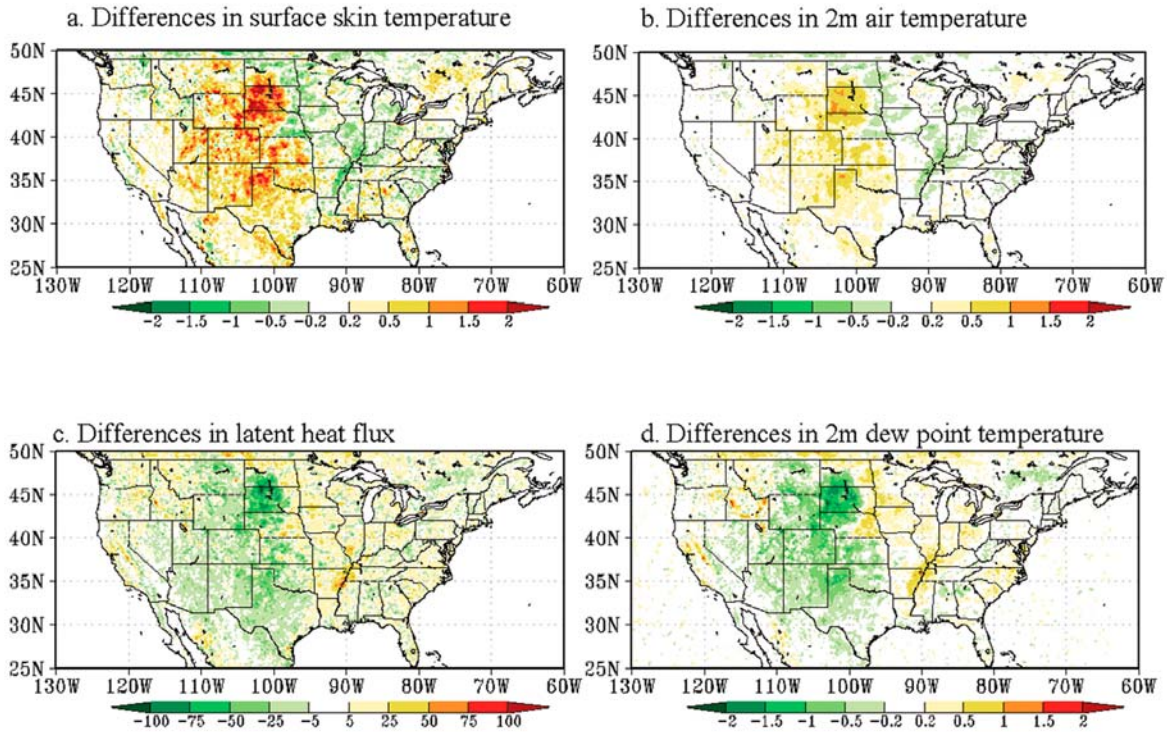

Figure 11. Surface differences (averaged from 17 model runs from 2 to 18 July 2006) by using the new real-time weekly GVF and using the new GVF weekly climatology after 33 h forecasts: (a) differences in surface skin temperature (unit: K); (b) differences in 2 m surface air temperature (unit: K); (c) differences in latent heat flux (unit: W m^{-2}); and (d) differences in 2 m dew point temperature (unit: K) (results by using the new real-time GVF minus results by using the new GVF climatology).

traceability to national or international standards defined physically. In an operational mode, it is critical to deliver real-time products shortly after the previous operational data stream, and it is difficult to acquire (in real time) adequate ancillary data required by most physics-based correction algorithms through operationally established procedures. Thus, mathematical and statistical smoothing and filtering were applied to the recalculated NDVI by post launch-calibrated GVI weekly composite AVHRR VIS and NIR channels. Such approaches are sound in terms of suppressing high-frequency noises (e.g., due to cloud contamination, short-term weather fluctuation, etc.) and removing the lumped effect of different physical contamination sources. They were proven effective in a wide range of applications and were the only feasible means of attaining reasonably estimated "ground truth" when none of spaceborne VIS and IR sensors can detect any ground signals under thick or persistent cloud cover. However, they make it impossible, after these mathematical adjustments, to trace back to different individual error sources explicitly. It must be also recognized that possible artifacts in the data products are introduced one way or another, depending on how the estimation approaches are applied.

[54] Note that the stabilized NDVI data set [*Jiang et al.*, 2008] is not claimed to be suitable as "climate data record" and appropriate for studying long-term global climate trends because of the nature of the corrections by the ACDF procedure, which assumed that the interannual global scale weekly NDVI to be stationary. In practice, the new GVF data set (derived from the ACDF-adjusted NDVI) can be treated as "consistent data record" rather than "climate data record. " It is achievable operationally and is suitable for use in NWPs, for example, to express regional GVF anomalies while climate data record is not easily achievable. The current development has provided a quality-improved long-term data set from the operational NOAA GVI data stream.

[55] The following limitations of the new weekly GVF data sets are also noted: (1) Given they are derived from the operational GVI products at NOAA/NESDIS, which only maps AVHRR data between 75°N and 55°S, it is not feasible currently to provide the true full global coverage required by GFS. (2) During the NH winter weeks, the high-latitude regions (i.e., northward of 60°N) are filled by a simple mathematical approach (assuming a simple vegetation growth/decay curve) due to the lack of reliable AVHRR data for these regions. (3) The GVF values in tropical areas may be undesirably low for some rainforest regions, such as Southeast Asia, North Africa, and the Amazon, due to persistent cloud, which could be longer than a few months because of the monsoon season. For such periods, there is no satellite observation for the surface under cloud cover, leaving relative large uncertainties for the GVF values. Currently, we are experimenting with different interpolation schemes for possible future enhancement while we do not have a solid approach to fix this issue. (4) Severe sensor-related issues and severe aerosol contamination issues are not fully addressed in the current global data sets. For example, several figures in

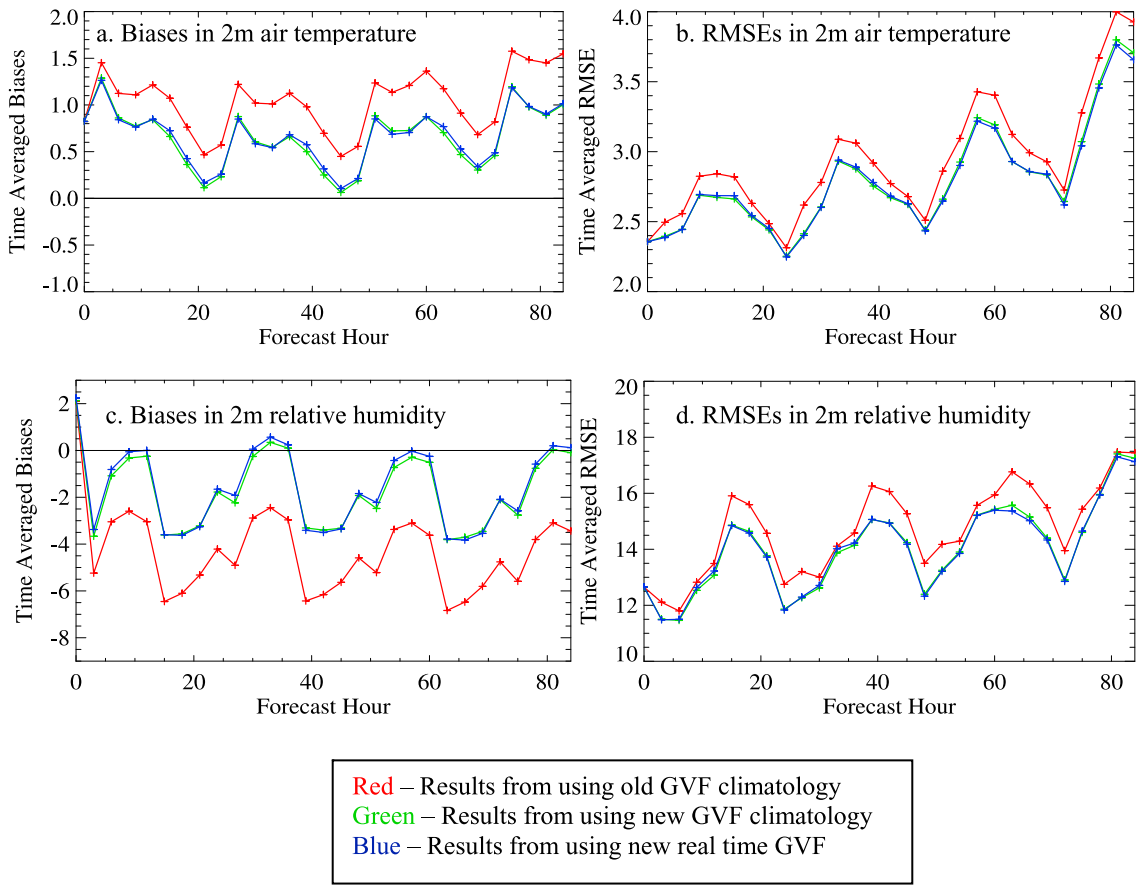

Figure 12. Comparison of errors in forecasts (averaged from 17 model runs from 2 to 18 July 2006) in surface air temperature and relative humidity: (a) bias in 2 m surface air temperature; (b) root mean square error (RMSE) of 2 m surface air temperature; (c) bias in 2 m relative humidity (%); and (d) RMSE in 2 m relative humidity (%).

this study show the very low mean GVF for a number of land types in 1991 (due to volcanic eruption) and 1994 (due to severe sensor degradation), implying further improvements are needed to explicitly account for these errors. Recent success by *Vargas et al.* [2009] using a more narrowed (instead of a global) empirical distribution function correction method is a step toward fixing such issues. (5) In addition, currently, we do not have a mature solar zenith angle effect correction module to apply to the weekly composite of AVHRR channel counts from GVI, from which the smoothed NDVI and GVF are derived.

6. Conclusion and Future Work

[56] This paper describes the operational algorithms used in the GVPS system to generate the real-time GVF data sets meeting the initial production needs with improved data quality.

[57] Detailed comparisons are made with the old 5 year monthly GVF climatology used in the operational weather and climate models at NCEP. We conclude that the new weekly GVF data set has significant advantages over the old 5 year monthly GVF climatology by (1) overall enhancement in spatial-temporal resolution, (2) overall improved representation of land surface green vegetation at varied land surface classes and locations, and (3) more importantly the real-time updated surface vegetation status increasingly needed by operational weather and forecasting models.

[58] The approach described in this study to derive GVF from NDVI is a direct linear scaling following *Gutman and Ignatov* [1998], while the scaling coefficients are slightly different. Such an approach has been justified from both theoretical and practical perspectives. The overall GVF data sets (including both 24 year climatology and real-time global GVF data reprocessed since week 35 of 1981), to a large extent, provide the improved and consistent quality while not claiming to be a climate quality product.

[59] Comparison with MODIS-based NDVIs at EOS land validation core sites and with GIMMS NDVI indicated the general agreement with MODIS product and less so with the GIMMS data set.

[60] Model impact studies using WRF-NMM (with the Noah LSM) demonstrated the surface fluxes terms and 2 m air temperature, etc., are sensitive to the use of the new GVF. Applications of the new GVF climatology data into the WRF-NMM model generally cools surface temperature over most regions compared to the old GVF climatology. The WRF-NMM simulations are also sensitive to the new GVF anomalies. Using the new real-time GVF data can either warm or cool surface temperature compared to the new climatology data, depending on the sign of GVF anomalies (negative or positive). Validated with the observations,

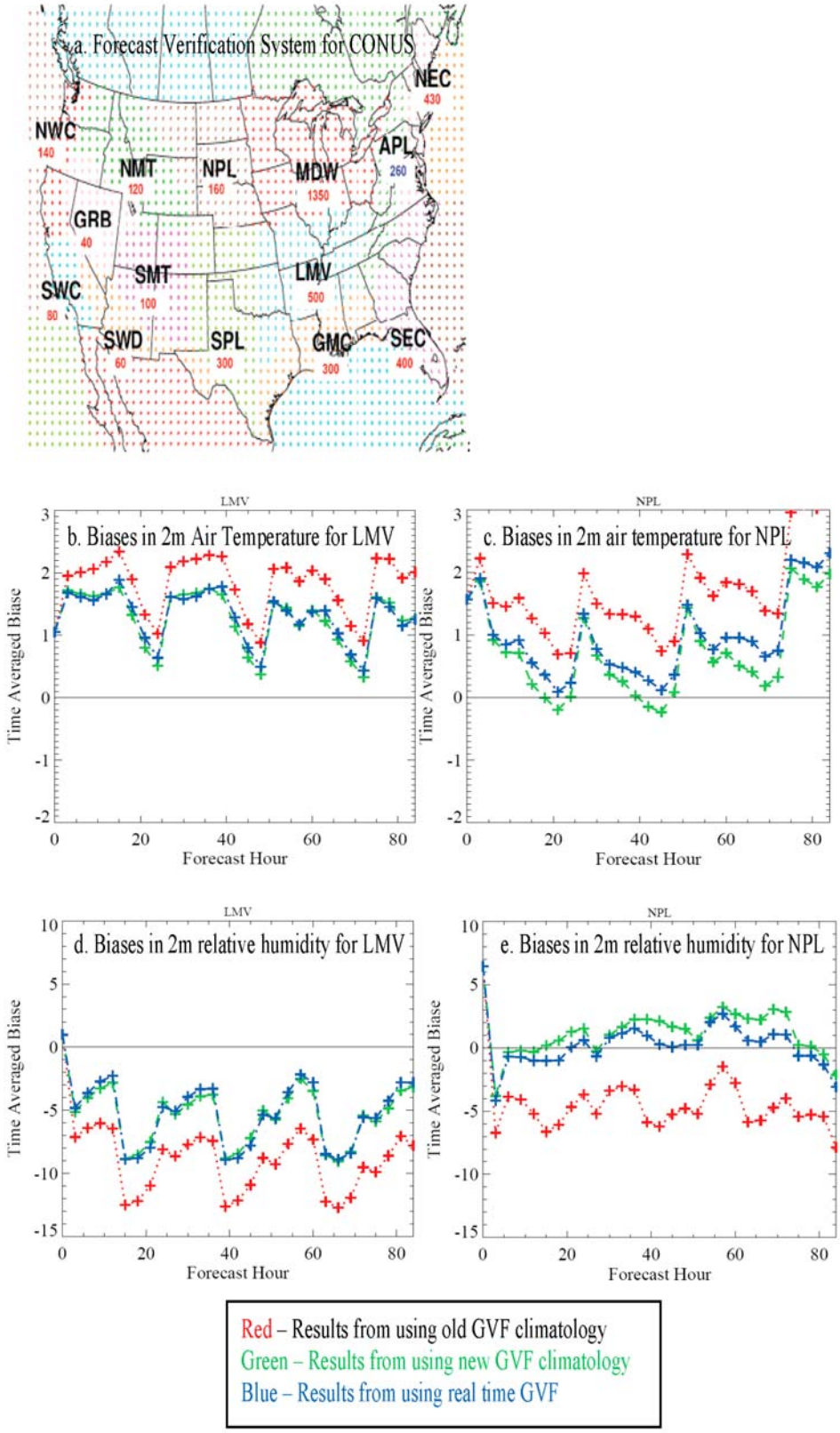

Figure 13. Forecast results (averaged from 17 model runs from 2 to 18 July 2006) verification over CONUS. (a) The 14 subregions in NCEP WRF-NMM forecast verification system. Number under each subregion name is the number of observation stations available to verify results every 3 h. (b) Bias in 2 m surface air temperature for LMV region. (c) Bias in 2 m surface air temperature for NPL region. (d) Bias in 2 m relative humidity (%) for LMV region. (e) Bias in 2 m relative humidity (%) for NPL region.

regional average biases for the 2 m surface air temperature and relative humidity show that the WRF-NMM using the old GVF data set has warm temperature biases and dry (negative) relative humidity biases during July 2006. Using both the new GVF data set (either the new climatology or real-time GVF) can significantly reduce the WRF-NMM surface warm biases.

[61] Currently, the operational GVPS run by NOAA/NESDIS/OSDPD generates weekly updated real-time global GVF product following routine schedules (e.g., in the late morning of each Monday) shortly after the GVI weekly production (i.e., weekly composite completed on Monday for the previous 7 days), and it has generated GVF products from week 35 of 1981 to present using GVI produced weekly channel counts from NOAA-7, NOAA-9, NOAA-11, NOAA-14, NOAA-16, NOAA-17, and NOAA-18. Data sets are available in both GRIB format and binary files. New modules are being implemented to process GVI output data stream based on the NOAA-19 (launched in February 2009) weekly composite as input to the GVPS in order to continuously generate GVF for use in the operational NWP models.

[62] In the long run, the operational production requirement shall not preempt feasible physics-based approaches to address various problems in the NOAA GVI products (used as inputs to the GVPS). As the overall operational capabilities evolve, future GVF enhancement cycles will consider transitioning a set of proven successful correction modules (such as solar zenith angle correction and physics-based atmospheric corrections, etc.) to the operational data product generation process.

[63] **Acknowledgments.** This work was funded by I. M. Systems Group, Inc. contract at NOAA/NESDIS/STAR (contract/task DG133E-06-CQ-0030/T004 and T020). We appreciate the assistance of Ivan Csiszar (NESDIS/STAR) for information on 5 year climatological GVF data and for his constructive comments during the manuscript revision; Ingrid Guch (NESDIS/STAR) and Hanjun Ding (NESDIS/OSDPD) for operational implementation suggestions; and Xiwu Zhan (NESDIS/STAR), Yunyue Yu (NESDIS/STAR), and Istvan Laszlo (NESDIS/STAR) for their insightful comments on an earlier version of the manuscript. Thanks are extended to Brad Ferrier (Science Applications International Corporation (SAIC) at NCEP/EMC), George Gayno (SAIC at NCEP/EMC), and Vince Wong (SAIC at NCEP/EMC) for providing the NCEP WRF-NMM code and incorporating the new GVF data into the model and to Hui-ya Zhuang and Binbin Zhou for providing helpful guidance in WRF-NMM postprocessing and forecast verification system, as well as to numerous peer reviewers during earlier submissions for their comments that helped improve the overall quality of this paper. The views, opinions, and findings contained in this work are of the author(s) and should not be interpreted as an official NOAA or U.S. Government position, policy, or decision.

References

Abramopoulos, F. (1988), Generalized energy and potential enstrophy conserving finite-difference schemes for the shallow-water equations, *Mon. Weather Rev.*, *116*(3), 650–662.

Belward, A. S. (1996), The IGBP-DIS global 1 km land cover data set (DISCover): Proposal and implementation plans, *IGBP-DIS Working Paper13*, 61 pp. [Available from IGBP-DIS Office, 42 Ave. Gustave Coriolis 31057 Toulouse Cedex, France.]

Betts, A, F. Chen, K. E. Mitchell, and Z. I. Janjic (1997), Assessment of the land surface and boundary layer models in two operational versions of the NCEP Eta model using FIFE data, *Mon. Weather Rev.*, *125*, 2896–2916.

Carlson, T. N., and D. A. Ripley (1997), On the relation between NDVI, fractional vegetation cover, and leaf area index, *Remote Sens. Environ.*, *62*, 241–252.

Carlson, T. N., E. M. Perry, and T. J. Schmugge (1990), Remote estimation of soil-moisture availability and fractional vegetation cover for agricultural fields, *Agric. For. Meteorol.*, *52*(1–2), 45–59.

Choudhury, B. J., N. U. Ahmed, S. B. Idso, R. J. Reginato, and C. S. T. Daughtry (1994), Relations between evaporation coefficients and vegetation indices studied by model simulations, *Remote Sens. Environ.*, *50*, 1–17.

Ek, M. B., K. E. Mitchell, Y. Lin, E. Rogers, P. Grunmann, V. Koren, G. Gayno, and J. D. Tarpley (2003), Implementation of Noah land surface model advances in the National Centers for Environmental Prediction operational mesoscale Eta model, *J. Geophys. Res.*, *108*(D22), 8851, doi:10.1029/2002JD003296.

Guo, W., and L. Jiang (2008), *Global Vegetation Processing System Users Manual* (version 4.0), 28 pp, NOAA/NESDIS/STAR, Camp Springs, Md.

Gutman, G., and A. Ignatov (1998), The derivation of the green vegetation fraction from NOAA/AVHRR data for use in numerical weather predication models, *Int. J. Remote Sens.*, *19*(8), 1533–1543.

Gutman, G., A. Ignatov, and S. Olson (1994), Towards better quality of AVHRR composite images over land: Reduction of cloud contamination, *Remote Sens. Environ.*, *50*, 134–148.

Huete, A. R., G. Hua, J. Qi, A. Chehbouni, and W. J. D. Vanleeuwen (1992), Normalization of multidirectional red and NIR reflectances with the SAVI, *Remote Sens. Environ.*, *41*(2–3), 143–154.

James, K. A., D. J. Stensrud, and J. Yussouf (2009), Value of real-time vegetation fraction to forecasts of severe convection in high-resolution models, *Weather Forecast.*, *24*(1), 187–210.

Jiang, L, J. D. Tarpley, K. E. Mitchell, S. Zhou, F. N. Kogan, and W. Guo (2008), Adjusting for long-term anomalous trends in NOAA's Global Vegetation Index data sets, *IEEE Trans. Geosci. Remote Sens.*, *46*(2), 409–422.

Kidwell, K. B. (1994), Global Vegetation Index User Guide, U.S. Dept. of Commerce, NOAA/NESDIS, Satellite Data Services Division, Nat. Climatic Data Center, Asheville, N. C.

Kidwell, K. B. (1997), NOAA Global Vegetation Index User's Guide (Revision), U.S. Dept. of Commerce, NOAA/NESDIS, Climate Services Division, Nat. Climatic Data Center, Suitland, Md.

Kogan, F. N. (1990), Remote sensing of weather impacts on vegetation in nonhomogeneous areas, *Int. J. Remote Sens.*, *11*(8), 1405–1419.

Kogan, F. N. (1997), Global drought watch from space, *Bull. Am. Meteorol. Soc.*, *78*, 621–636.

Kogan, F. N. (2001), Operational space technology for global vegetation assessment, *Bull. Am. Meteorol. Soc.*, *82*(9), 1949–1964.

Kurkowski, N. P., D. J. Stensrud, and M.E. Baldwin (2003), Assessment of implementing satellite-derived land cover data in the Eta model, *Weather Forecast.*, *18*, 404–416.

Miller, J., M. Barlage, X. Zeng, H. Wei, K. Mitchell, and D. Tarpley (2006), Sensitivity of the NCEP/Noah land surface model to the MODIS green vegetation fraction data set, *Geophys. Res. Lett.*, *33*, L13404, doi:10.1029/2006GL026636.

Mitchell, K. E., et al. (2004), The multi-institution North American Land Data Assimilation System (NLDAS): Utilizing multiple GCIP products and partners in a continental distributed hydrological modeling system, *J. Geophys. Res.*, *109*, D07S90, doi:10.1029/2003JD003823.

Myneni, R. B., C. D. Keelivolng, C. J. Tucker, G. Asrar, and R. R. Nemani (1997), Increased plant growth in the northern high latitudes from 1981 to 1991, *Nature*, *386*, 698–702.

Pedelty, J., et al. (2007), Generating a long-term land data record from the AVHRR and MODIS instruments, *IEEE Int. Geosci. Remote Sens. Symp.*, Barcelona, Spain, July 2007.

Pinzon, J., M. E. Brown, and C. J. Tucker (2005), Satellite time series correction of orbital drift artifacts using empirical mode decomposition, in *Hilbert-Huang Transform*, edited by N. Huang, *Intro. Appl.*, 167–186.

Rao, C. R. N., and J. Chen (1995), Inter-satellite calibration linkages for the visible and near-infrared channels of the advanced very high resolution radiometer on the NOAA-7, -9, and -11 spacecraft, *Int. J. Remote Sens.*, *16*, 1931–1942.

Roujean, J. L., M. Leroy, and P. Y. Deschamps (1992), A bidirectional reflectance model of the Earth's surface for the correction of remote sensing data, *J. Geophys. Res.*, *97*(D18), 20,455–20,468, doi:10.1029/92JD01411.

Seiler, R. A., F. N. Kogan, and W. Guo (2000), Monitoring weather impact and crop yield from NOAA AVHRR data in Argentina, *Adv. Space Res.*, *26*(7), 1177–1185.

Tarpley, J. D., S. R. Schneider, and R. L. Money (1984), Global vegetation indices from NOAA-7 meteorological satellite, *J. Clim. Appl. Meteorol.*, *23*, 491–494.

Tian, Y., C.-Z. Zou, K. E. Mitchell, V. Wong, F. N. Kogan, L. Jiang, and X. Zhan (2008), Improvements of numerical weather predictions using

a new AVHRR green vegetation fraction dataset, *Atmospheric and Environmental Remote Sensing Data Processing and Utilization IV: Readiness for GEOSS II, Proc. SPIE*, *7085*, doi:10.1117/12.795316.

Tucker, C. J., J. E. Pinzon, M. E. Brown, D. Slayback, E. W. Pak, R. Mahoney, E. Vermote and N. El Saleous (2005), An Extended AVHRR 8-km NDVI data set compatible with MODIS and SPOT Vegetation NDVI Data, *Int. J. Remote Sens.*, *26*(20), 4485–5598.

Ulanova, E. S. (1975), Climate and winter wheat yield, *Hydrometizdat*, 298 pp.

Vargas, M., F. Kogan, and W. Guo (2009), Empirical normalization for the effect of volcanic stratospheric aerosols on AVHRR NDVI, *Geophys. Res. Lett.*, *36*, L07701, doi:10.1029/2009GL037717.

Vermote, E. F., N. El Saleous, C. O. Justice, Y. J. Kaufman, J. L. Privette, L. Remer, J. C. Roger, and D. Tanre (1997), Atmospheric correction of visible to middle-infrared EOS-MODIS data over land surfaces: Background, operational algorithm and validation, *J. Geophys. Res.*, *102*(D14), 17,131–17,141.

Zeng, X., R. E. Dickinson, A. Walker, M. Shaikh, R. S. DeFries, and J. Qi (2000), Derivation and evaluation of global 1-km fractional vegetation cover data for land modeling, *J. Appl. Meteorol.*, *39*, 826–839.

Zeng, X., P. Rao, R. S. DeFries, and M. C. Hansen (2003), Internannual variability and decadal trend of global fraction vegetation cover from 1982 to 2000, *Notes and Correspondence, J. Appl. Meteorol.*, *42*, 1525–1530.

W. Guo, L. Jiang, and Y. Tian, I. M. Systems Group, Inc., National Environmental Satellite, Data, and Information Service, NOAA, 5200 Auth Rd, Rm 710, Camp Springs, MD 20746, USA. (le.jiang@noaa.gov)

F. N. Kogan, B. H. Ramsay, J. D. Tarpley, and C.-Z. Zou, National Environmental Satellite, Data, and Information Service, Center for Satellite Applications and Research, NOAA, World Weather Building, Science Center, Room 707, 5200 Auth Road, Camp Springs, MD 20746, USA.

M. B. Ek and K. E. Mitchell, National Centers for Environmental Prediction, Environmental Modeling Center, NOAA, 5200 Auth Road, Camp Springs, MD 20746, USA.

W. Zheng, Science Applications International Corporation, National Centers for Environmental Prediction, Environmental Modeling Center, NOAA, 5200 Auth Road, Camp Springs, MD 20746, USA.